Bacterial cellulose-graphene oxide composite membranes with enhanced fouling resistance for bio-effluents management

Check for updates

Ishfaq Showket Mir[1,2] ✉, Ali Riaz[3], Julie Fréchette [3], Joy Sankar Roy[3], James Mcelhinney [2], Sisi Pu[2,4], Hari Kalathil Balakrishnan[2,4], Jesse Greener[1], Ludovic F. Dumée[2,4] ✉ & Younès Messaddeq[3]

Bacterial cellulose composites hold promise as renewable bioinspired materials for industrial and environmental applications. However, their use as free-standing water filtration membranes is hindered by low compressive strength, fouling, and poor contaminant selectivity. This study investigates the potential of bacterial cellulose-graphene oxide composites membranes for fouling resistance in pressure-driven filtration. Graphene oxide dispersed in poly(ethylene glycol) (PEG-400) is incorporated as a reinforcing filler into 3D network of bacterial cellulose using an in-situ synthesis method. The effect of graphene oxide on in situ fermentation yield and the formation of percolated-network in the composites shows that the optimal membrane properties are reached at a graphene oxide loading of 2 mg/mL. The two-dimensional graphene oxide nanosheets uniformly dispersed into the matrix of bacterial cellulose nanofibers via hydrogen-bonded interactions demonstrated nearly twofold higher water flux (380 L m^{-2} h^{-1}) with a molecular weight cut-off ranging between 100–200 KDa and a sixfold increase in wet compression strength than pristine BC. When exposed to synthetic organic foulants and bacterial rich feed solutions, the composite membranes showed more than 95% flux recovery. Additionally, the membranes achieved over 95% rejection of synthetic natural organic matter and bacterial rich solutions, showcasing their enhanced fouling resistance and selectivity.

In response to the growing global concerns of water pollution, plastic waste, and energy shortages, there is a pressing need for the development of eco-friendly fabrication techniques for renewable bio-based materials. Biode-gradable biopolymers, including polyesters (such as polyhydroxyalkanoates (PHA), polylactide (PLA), and polyethylene furanoate (PEF)), poly-saccharides (such as cellulose, chitin, and alginate), and polyamides (such as γ-poly (glutamic acid) (PGA), silk, and collagen) are garnering increasing attention due to their potential in addressing these challenges[1]. Bacterial cellulose (BC), a biopolymer produced by microbes, has recently gained significant interest from academic and industry experts. Biosynthesis of BC relies on glucose, fructose, and glycerol as preferred carbon sources. The formulation of the nutrient medium and culture conditions, such as shaking or static culture, significantly influence BC production, morphology of the fibers and network assembly. Shaking cultures favor efficiency, while static cultures maintain genetic stability and provide membranes with the high quality, size and shape which are crucial for applications like water treatment[2,3].

BC possesses unique structural and physicochemical properties such as flexibility and tensile strength (Young Modulus of 15–18 GPa), water holding capacity (over 100 times of its own weight), high surface area (high aspect ratio of fibers with diameter 20–100 nm), ease of functionalization, and permeability to gases and water[4–6]. These versatile properties make BC suitable for a wide range of applications including medical uses, such as artificial skin, wound dressings, and substrates in drug delivery systems, and in various industries like food, paper, textiles, and electronics[7,8]. However, the use of pure BC as a membrane for pressure-driven filtration is not widely

[1]Département de Chimie, Faculté des Sciences et de Génie, Université Laval, Québec, QC, Canada. [2]Department of Chemical and Petrochemical Engineering, Khalifa University, Abu Dhabi, United Arab Emirates. [3]Centre d'Optique, Photonique et Laser (COPL), Université Laval, Québec, QC, Canada. [4]Research and Innovation Center on 2D Nanomaterials (RIC2D), Khalifa University, Abu Dhabi, United Arab Emirates. ✉e-mail: ishfaq-showket.mir.1@ulaval.ca; Ludovic.dumee@ku.ac.ae

adopted due to its limitations, such as a lower compressive strength, a lower permeance, and minimal pollutant retention. The presence of only –OH groups in the native structure of BC and lack of antibacterial property limit the diversity of interactions available for repelling and microbial foulants and hence contribute to its higher susceptibility to fouling[9,10]. Dehydration of BC induced by evaporation and compressive stress results in fiber stacking, which leads to collapsing of open pores permanently and reducing flux in pressure-driven filtration systems, thus increasing operational costs. BC membrane is an ideal structure to build on the desirable membrane properties as the biosynthesis of BC involves formation of some straight through channels due to the natural and complex formation of loose fibers in the Z-direction. The abundance of hydroxyl groups in BC facilitates the formation of hydrogen bonding, resulting in the formation of dense layers[11]. However, the interlayer distance formed during biosynthesis of BC due to natural stacking of dense fiber layers obstructs the formation of straight-through passages in the Z direction of the membrane. This results in lower compression strength and higher resistance to fluid permeance through the membrane. To address these issues, adding a reinforcing filler like graphene oxide (GO) to the BC membrane was considered to enhance its resistance to compression stress. GO is among the well-known materials owing to its multifunctional properties. These include high surface area[12] ($2600 \, m^2g^{-1}$), favorable physicochemical and mechanical properties[13] (Young modulus of 300 GPa) and ultrafast transport capabilities[14] ($71 \, LMH \, bar^{-1}$) due to the presence of several oxygen containing functional groups such as hydroxyls, epoxy, carboxyl and carbonyl groups[15].

Increasing the number of pores and reducing the actual capillary tube length enhances membrane permeability[16]. To achieve this, more pores should be incorporated in the X-Y direction during BC biosynthesis, with fibers loosely oriented in the Z direction. The addition of a porogen can both enhance the membrane's pore count in the X-Y direction and inhibit layer stacking in the Z direction during fiber biosynthesis. The addition of porogen such as Ca-alginate and paraffin wax during BC biosynthesis enhances pore count and inhibits Z-directional layer stacking but decreases membrane fineness and poses challenges in porogen removal post-harvesting[17]. PEG is an alternative porogen that exhibits chain mobility, an excluded volume effect, high-water content, and low interfacial free energy. PEG is a hydrophilic polymer widely used as an additive for morphology control and increasing the water flux and fouling resistance[18]. These properties facilitate the formation of a protective layer on surfaces, rendering it an adept choice for fouling resistance. Additionally, its weakly basic ether linkages deter protein adhesion and generate nano-sized pores, creating ideal conditions to enhance membrane flux[19].

Most of the techniques proposed to develop BC as a filter membrane have involved the use of toxic or expensive chemicals such as poly(hexamethylene guanidine hydrochloride)[20,21], complex processes such as sulfonation, TEMPO-mediated oxidation, phosphorylation[22] or inadequate porogen removal[23] to achieve desired properties. Most of the methods employed involve defibrillating the native fibrillar structure that leads to compromise the innate properties of BC[24]. Enhancing BC compression strength have been explored by methods such as cross-linking and chemical modification, exemplified by the use of agents like epichlorohydrin and glutaraldehyde. Despite efficacy, their acute toxicity necessitates rigorous washing protocols to remove residual substances[25–28].

To address the above challenges, this study explores the in-situ approach for synthesizing BC-GO composite membranes with optimized wider pore distribution, mechanical stability in hydrated state and anti-fouling behavior for pressure driven water filtration applications. A novel approach to incorporate GO into the 3D network of BC in situ was also developed, enabling uniform GO distribution all over the surface and precise control over the design of thin film membrane properties.

Methods
Chemicals and materials
The cellulose producing strain *Komagataeibacter hansenii* (ATCC 53582) was procured from American Type Culture Collection (ATCC), Canada in a frozen vial. The vial was stored at −80 °C until further use. *E. coli* strain DH5α was purchased from Microbiologics (Kwik Stik format). The nutrient components for Hestrin−Schramm (HS) growth medium consisting of peptone, yeast extract, disodium hydrogen phosphate, citric acid, and glucose were purchased from Nzytech, HilMedia, Glentham and Sigma-Aldrich. PEG and PEO (poly(ethylene oxide) of different molecular weights, humic acid (HA; technical grade), sodium alginate (SA) and bovine serum albumin (BSA; 66 KDa) were purchased from Acros Organics and Sigma-Aldrich. Graphite powder was obtained from Asbury Graphite Mills, USA. Sodium nitrate ($NaNO_3$), potassium permanganate ($KMNO_4$; 99%), sulfuric acid (H_2SO_4; 96%), hydrochloric acid (HCl; 36.5% w/w), sodium hydroxide (NaOH) and hydrogen peroxide (H_2O_2, 30% v/v aqueous solution), and absolute ethanol (C_2H_5OH; 99.95%) were purchased from Sigma-Aldrich. The petri-dishes (Huanyu; Borosilicate glass; diameter of bottom dish: 120 mm; height of bottom dish: 27 mm; outer diameter of Upper Lid: 132 mm; height of upper Lid: 27 mm; thickness: 2 mm) used to grow the membranes were bought from Amazon.

Microorganisms revival procedure
The sample from the ATCC thawed vial was revived following ATCC protocol[29]. After opening the vial, the entire content was transferred aseptically into a 10 mL tube containing sterile HS medium (ATCC-1765) with $5.0 \, g \, L^{-1}$ peptone, $5.0 \, g \, L^{-1}$ yeast extract, $2.5 \, g \, L^{-1}$ disodium hydrogen phosphate, $1.5 \, g \, L^{-1}$ citric acid, and glucose $20 \, g \, L^{-1}$ with pH adjusted to 5.4. Secondary test tubes were inoculated by transferring 1 mL from the primary test tube. To prepare a stock culture, several drops from the primary tube were used to inoculate the ATCC recommended 1765 agar plates. The tubes and the agar plates were incubated at 26 °C for 4 days and then used for further studies. The agar plates were stored at 4 °C until further use.

E. coli cultures were initiated from frozen stocks stored in 30% glycerol at −80 °C. These were handled swiftly to prevent thawing and manipulated in aseptic conditions. They were streaked onto a Luria-Bertani (LB) agar plate using a sterile applicator stick and incubated overnight at 37 °C to obtain isolated colonies. For bacterial quantification, 10-fold serial dilutions of overnight cultures were prepared and 100 μL from each was spread onto agar plates. These were incubated overnight at 37 °C. Bacterial concentrations on the order of $1 \times 10^8 \, CFU/mL$[29] were targeted for inoculation of *E.coli*.

Synthesis and characterization of graphene oxide nano-sheets
GO nano-sheets were synthesized from graphite powder using modified Hummer's method[15,30]. Briefly, graphite (2 g) was added to 250 mL of H_2SO_4 (98%) stirred for 1 h at 25 °C, followed by the gradual addition of 10 g $KMNO_4$ and stirred for 24 h. After transferring to an ice bath, 100 mL H_2O_2 (30%) and 500 mL DI water were added, turning the mixture golden yellow. The solution was centrifuged, treated with 10% HCl, washed several times to pH ≥ 5, and the resulting gray paste was dried for storage.

ATR-FTIR spectra of GO were recorded and depicted in Supplementary Fig. 1. GO dispersions were prepared in DI water. In a typical process, 20 mL of an aqueous GO suspension at concentrations of 0.5, 1, 2, 10, 30 and 50 mg/mL was sonicated and then subjected to intense mechanical stirring for 60 min. Then the dispersions were left at room temperature without stirring to remove any trapped air bubble. GO dispersions were sterilised by rinsing in ethanol under sterile conditions[31]. They were then allowed to dry into a biosafety cabinet before being suspended into 6 mL of PEG-400 at concentrations of 0.5, 1, 2, 10, 30 and 50 mg/mL. The mixture was sonicated for 1 h followed by intense mechanical stirring for 60 min which resulted in the formation of stable dispersions of GO.

In-situ synthesis of BC-GO composite membranes
The HS medium, adjusted to a pH of 5.4, was prepared and autoclaved at 121 °C for 15 min. Sterile glass Petri dishes, each with a diameter of 120 mm, were used to grow the composite membranes as shown in Supplementary Fig. 3. 150 mL of HS medium inoculated with 4-day pre-grown cultures of *K. Hansenii* at a ratio of 1:15 was poured in each Petri dish. In the first set of

experiments, 10 mL of GO dispersions in DI water at different concentrations (0.5, 2, 30 and 50 mg/mL) were added to the inoculated Petri dishes. In the second set of experiments, 10 mL of GO dispersions in PEG-400 at the same concentrations (0.5, 2, 30 and 50 mg/mL) were added to the inoculated Petri dishes. The inoculated petri dishes were labeled and statically incubated at 26 °C. Samples were collected after time intervals of 2, 4, 6, 8, 10, 12, 14 and 16 days to analyze the BC production yield. A control experiment, without GO during BC biosynthesis, was performed in parallel. All the experiments were performed at least in triplicate, and results correspond to averages with standard deviations.

Purification and quantification of BC-GO composites

BC-GO composite membranes were isolated from HS media using sterile forceps and pressed to extrude the extra liquid. To remove the bacterial cells from the BC-GO composite membranes, they were first rinsed with DI water, then treated with 0.1 M NaOH at 80 °C for 90 min. Membranes were rinsed several times with refreshed DI shaking baths until a pH of 7 was obtained[9]. For yield analysis, pristine-BC and BC-GO membranes were air-dried in an oven at 40 °C for 3 days. The mass of the BC-GO composites collected after different incubation periods was measured using a precision balance. The BC-GO films were kept in a desiccator for future investigations.

Determination of BC yield

The optical density at 600 nm (OD_{600}) of the inoculum used to synthesize BC-GO composites was measured (using UV−Visible spectrophotometer, Thermo scientific Genesys, 10S) and kept constant for each study batch. This was done to ensure repeatability of the process.

To explore the effects of different GO concentrations in the nutrient medium and the optimized incubation duration, the yield of BC production was calculated. The dry weight (40 °C until constant weight) of in situ produced BC-GO was measured to determine its yield. BC production was recorded as the dry weight of cellulose obtained per volume of medium (g/L). Equation (1) was used to calculate the production yield.

$$\text{Yield}\,(\%) = \frac{m\text{BC dry}}{m\text{Carbon source}} \tag{1}$$

Here, mBC dry is dry weight of the BC membrane (g) and mCarbon source is the initial weight of carbon source (e.g., glucose or glycerol) in the medium (L).

Characterization of BC-GO composite membranes

The morphology of the top surface of the dried pristine and BC-GO composite membranes was examined with an FEI Nova NanoSEM 650 Scanning Electron Microscope (SEM) with monopole magnetic immersion final lens and 60° objective lens geometry at an electron beam energy of 5 kV, emission current of 100 µA, and chamber vacuum <10 mPa. To obtain the cross-sectional images, the membranes were kept in liquid nitrogen for 30 s and then fractured gently. Before analysis, a 7 nm layer of gold was deposited on the surface of the samples to maximize conductivity and improve SEM analysis.

The pore size distribution of the never dried pristine-BC and BC-GO composite membranes was studied using the Molecular Weight Cut-Off method (MWCO), defined as the molecular weight of solutes at which solute rejection reaches 90%. Rejection tests were conducted using PEG and polyethylene oxide (PEO) solutes with a concentration of 200 ppm in DI water. The tests were performed with PEG and PEO solutes having molecular weights (MW) of 10,000; 20,000; 35,000; 90,000; 100,000; 200,000 and 300,000 g/mol under the operating pressure of 2 bar at 25 °C in a cross-flow filtration setup, as shown in Supplementary Fig. 2[32]. Solutes were filtered for 1 h and % rejection was calculated, with the use of a TOC analyzer (SCHIMADZU Corporation, TOC-L CSH).

The Stokes radius r_s(nm) of the PEG and PEO solutes were calculated based on their molecular weights from Eqs. (2) and (3) respectively:

$$\text{PEG}\, r_s = 16.73 \times 10^{-2} \times MW^{0.557} \tag{2}$$

$$\text{PEO}\, r_s = 10.44 \times 10^{-2} \times MW^{0.587} \tag{3}$$

Plotting solute rejection against the Stokes diameter of PEG and PEO in a log-normal probability plot, a straight line and a linear equation can be obtained via curve fitting. From Eqs. (2) and (3), the average effective pore size of the never dried membranes could be obtained. Ignoring the steric and hydrodynamic interactions between solutes and pores, the mean pore size (r_p) and the geometric standard deviation of the effective pore size are the same. The pore size distribution of the membranes can be deduced according to the following probability density function[33].

$$\frac{dRs\,(r_p)}{dr_p} = \frac{1}{d_p \ln\sigma_p \sqrt{2\pi}} \exp\left[-\frac{\left(\ln d_p - \ln\mu_p\right)^2}{2\left(\ln\sigma_p\right)^2} \right] \tag{4}$$

where μ_p is the mean effective pore size which is determined with the solute rejection Rs = 50%, and σ_p is the geometric standard deviation which is defined as the ratio of d_p at Rs = 84.13% over that at R = 50%.

The physicochemical characterization of the BC-GO composites was conducted using Fourier transform infrared (FTIR) spectroscopy (PerkinElmer, Frontier). Composite films were placed on a ZnSe crystal and analyzed. Spectra were recorded in the 4000–500 cm^{-1} wavenumber range at a resolution of 4 cm^{-1} with 32 scans taken to obtain the ATR-FTIR spectra.

The Raman spectra were acquired with a WI Tec's Alpha 300 R confocal micro-Raman imaging spectrometer with a visible laser excitation source at 532 nm. The spectra were recorded over six different points with accumulations of 10 and acquisition time of 20 s for each spectrum.

The thermal characteristics of BC-GO composite membranes were measured using Thermogravimetric analysis (TGA) (NETZSCH High Temperature TGA) with a platinum crucible under inert settings. BC-GO membranes (2–5 mg) were heated 20 °C to 800 °C at a rate of 10 °C/min with nitrogen gas flow (30 mL/min).

The streaming potential of the BC-GO composite membranes was determined with a SurPASS3 (Anton Paar GmbH) Electrokinetic Analyzer having an adjustable gap cell (20 × 10 mm) with pressure vessel volume and fill volume of 0.00235 m³ and 0.0001 m³ respectively. The background solution included 10 mM KCl, and the starting pH was 2. To adjust pH, appropriate amounts of 0.1 M KOH were dosed automatically into the tested solution. Three washing cycles and four zeta potential measurements with a pressure of 400 mbar and flow rate of 500 mL/min were performed for each pH.

The static contact angles of BC-GO composite membranes were determined using the sessile drop technique on a Krüss GmbH drop shape analyzer, DSA25, with 5 µL DI water droplets ejected by a micro-syringe. Measurements were taken over five distinct surface areas, and average results were reported.

Compression measurements for BC-GO composites were conducted on an advanced rotational rheometer (HAAKE Mars III Rheometer, Thermo Fisher Scientific, Karlsruhe, Germany) with a heat adjustable Peltier element at a temperature of 25 °C. Parallel plates of 25 mm diameter were used after coating a fine emery paper to improve adhesion (P240/S85, 58 µm roughness). For each experiment, the initial gap corresponding to the distance between the top and bottom plates, was adjusted according to the sample thickness. The behavior under compression was studied at a strain rate of 100 µm/s to investigate the response of the composites under compression. Samples were compressed from their initial thickness to the narrowest possible gap (typically 300–500 µm) achievable within the

constraints of the normal force transducer (50 N) of the instrument. Between 5 and 8 replicates were measured.

The porosity of pristine-BC and BC-GO composites was determined using the gravimetric method. Membranes were cut into equal circles, soaked in DI water for 24 h, then weighed. After weighing, they were dried according to the method described in section "Purification and quantification of BC-GO composites" and their dry weight was recorded. Membrane thickness was measured using a digital micrometer (Mitutoyo, Japan). Porosity was calculated using Eq. (5)

$$\varepsilon = \frac{Wwet - Wdry}{A.mt.\rho_g} \qquad (5)$$

where ε is the porosity (%), Wwet and Wdry are the wet and dry weights (g), A is the membrane area (cm^2), mt is the measured membrane thickness (cm), ρ_g is the DI water density at T = (0.998 g.cm^{-3}).

Membrane filtration performance

A cross-flow filtration setup designed in lab and equipped with a commercial cross-flow filtration cell (Sterlitech, CF042 Cell, Acetal Copolymer (Delrin) (CF042D), as shown in Supplementary Fig. 2, was used to evaluate membrane performance under pressure. It should be noted that for all filtration tests, never dried pristine-BC and BC-GO composites with a thickness of 1.2 mm were used. At lower thicknesses than 1.2 mm, the membrane is not considered to be self-standing, which makes it more difficult to handle. A wet thickness of around 1.2 mm is considered to exhibit maximum flow and stability. The effective filtration area of the membranes used was 42 cm^2, determined by the holder aperture. Prior to filtration, membranes were compacted for 30 min at a pressure of 2 bar. The evaluation of membrane's stability in flux was conducted by recording the Pure Water Flux (PWF) variations over different pressures ranging from 0.1 to 3.0 bar. Subsequently, experiments were performed under the established stable conditions of flux and pressure, ensuring consistency in performance throughout the study. The volume of DI water collected on the permeate side after 1 h was measured. Five filtration cycles, each lasting for 1 h, were run with pure water for pristine-BC and BC-GO composite membranes. PWF (J_w) (LMH) was calculated using Eq. (6).

$$J_w = \frac{V}{A \times t} \qquad (6)$$

where V is the volume of permeate (L), A is the effective filtration area (m^2) and t is the filtration duration (h).

To assess the anti-fouling performance of pristine-BC and BC-GO composite membranes, synthetic NOM solution mimicking the foulants present in wastewater was synthesized. The foulant solutions were prepared by dissolving the appropriate amount of BSA, SA and HA to yield a 100-ppm solution in 10 mM phosphate buffer solution (pH = 7) for BSA and in DI water for SA. For HA, 100 ppm HA solution was prepared by dissolving HA in 0.1 M NaOH solution, followed by pH reduction to 7 by adding 0.5 M HCl solution[34].

The Natural Organic Matter (NOM) synthetic solution was used to evaluate membrane antifouling properties. The NOM solution was used as a feed solution and kept under agitation using a magnetic stirrer so that the larger foulants do not settle at the bottom of the feed tank. In the first set of filtration cycles, the 200 ppm NOM solution was run for 5 h in the cross-flow assembly. After every 1 h of filtration with NOM, the membranes were cleaned by shear in the crossflow cell using DI water. The cleaning of the membranes was followed by recording the PWF for 1 h and then again feeding NOM. This cleaning and fouling operation continued for five cycles. In the second set of filtration cycles, the same procedure was adopted except that instead of DI water, 0.05 M NaOH solution was used as a cleaning solution. The NOM content in the feed and permeate solutions was determined by TOC analyzer using a non-dispersive infra-red detector (NDIR) with a supply gas pressure of 254.0 Kpa and carrier gas flow rate of 150 mL/min. The furnace temperature was maintained at 681 °C and NDIR temperature set at 65.4 °C. The rejection of NOM was calculated with Eq. (7).

$$R = 1 - \left(\frac{C_p}{C_f}\right) \times 100\% \qquad (7)$$

Where C_p and C_f are the TOC concentrations in the permeate and feed solutions, respectively. The flux recovery ratio (FRR) was calculated using Eq. (8).

$$FRR\,(\%) = \frac{J_{w_n}}{J_{w_{n-1}}} \times 100\% \qquad (8)$$

Where J_{wn} and J_{wn-1} is the water flux in the nth cycle and (n-1)th cycle (LMH) respectively.

In the next stages of filtration, the membranes were evaluated for the removal of microbial pollutants (E. coli) from model wastewater. The cross-flow filtration mode was also used for the filtration of bacteria, with the exception that the feed and permeate vessels were jacketed to regulate temperature. Before testing, the filter cell was rinsed in an aqueous solution of sodium chlorate (1000 ppm) for 30 min to ensure that all bacteria were removed. It was then repeatedly washed with deionized water. All the glassware was sterilised at high pressure and elevated temperature (120 °C, 198 kPa) for 15 min. Tests for bacterial retention were conducted at room temperature (22–24 °C). The plate counting method was used to determine the bacterial concentration. This procedure involved uniformly spreading 100 μL of produced dilutions onto LB solid medium, which was then cultivated for 18 h at 37 °C in a temperature incubator. After 18 h, pictures were taken to record the number of colonies. From these plates, bacterial culture was standardized to minimize the impact of changes in bacterial physiology on outcomes. The filtration lasted for five cycles with intermediate cleaning in between the cycles with DI water. Permeate was collected after every hour. The biofouling pattern of the membranes was followed by recording the PWF and flux decline when bacterial broth was fed to the membrane. The rejection of E. coli from permeates and feed samples were analysed by flow cytometer (FCM).

FCM samples were stained according to the standardized protocol proposed in the EAWAG, switzerland[35]. Intact (ICC) and membrane-compromised (MCC) cell counts for E. coli populations in feed and permeate waters were determined by dual staining with propidium Iodide (PI, Sigma Aldrich, UK) and SYBR Green 1 (SG, Sigma Aldrich, UK). Intermediate dual-staining stock solutions (DS) of 100 × SG and 600 μM PI were prepared from master stocks by dilution in 10 mM 0.22 μm filtered TRIS (pH 8.1). 5 μL of intermediate stock was added to 495 μL of sample to bring the final stain concentrations to 1 × and 6 μM (for SG and PI, respectively). For unstained control samples, 5 μL of 0.85% w/v NaCl (sterile filtered) was used in place of DS, to bring to the same final volume as stained samples (500 μL). Samples were briefly vortexed and incubated at 30 °C in the dark for 20 min with gentle mixing on an orbital shaker (at 110 RPM). Once stained, samples were immediately queued for acquisition on an Accuri C6+ (BD, USA). A threshold of 12,000 on FSC-H was used, based on optimization tests using E. coli, carried out previously by our group. Samples were acquired using a flow rate of 35 μL min^{-1}, with a core size of 16 μm and a sample acquisition volume limit of 50 μL. SG fluorescence was captured in FL1-H (533/30 nm) and PI was captured in FL3-H (670 LP). Samples were diluted, prior to staining, based on initial pre-run tests to ensure counts were kept below 4000 events/μL. FCM data processing was carried out using computational FCM workflows, essentially as described previously[36]. Briefly, FCS files describing FCM datasets were read into RStudio using the FlowCore package[37]. Flowset expression data were transformed by logical transformation in FlowCore and population statistics were calculated using a user defined gating template, shown in Supplementary Fig. 4 for computational gating as part of the OpenCyto package[38] to mitigate against

idiosyncratic artefacts associated with traditional manual gating. Statistical contrasts between membrane types were carried out in R[39] within RStudio[40] using 1- and 2-way ANOVA tests as implemented in the *stats* package in R.

The bacterial retention efficiency of the membranes was calculated in terms of LRV (Log reduction values) defined in Eq. (9).

$$LRV = log \frac{C_o}{C_p} \tag{9}$$

Where C_o and C_p are the concentrations of feed and permeate solution, respectively.

Results and discussion

The discussion first addresses the controlled in-situ synthesis of BC-GO membranes and the impact of varying GO concentrations on BC yield, elucidated in terms of wet thickness over different incubation periods. Subsequent sections cover membrane morphology and physicochemical properties, followed by an evaluation of the filtration capabilities, including permeance, fouling behavior and rejection of microbial pollutants.

In-situ biosynthesis of BC-GO composite membranes

In-situ bio fabrication of BC composites, which involves adding components directly into the nutrient medium, is an effective approach for incorporating new elements into the BC network[2,41]. Water-soluble polymers are commonly utilized in static in situ BC fermentation because they mix well with the nutrient medium and become confined within the BC network. Incorporating inorganic particles into the BC network is challenging due to their instability in ionic strength needed for bacterial fermentation[42]. The in situ agitated biosynthesis technique appears as an effective method to suspend inorganic particles uniformly in the nutrient medium which facilitates their incorporation into the BC network during fermentation. However, this method typically produces only small spherical BC membranes less than 1 cm in diameter, which are more likely to disperse into the entire medium volume rather than being incorporated into the BC network[43,44]. To overcome these challenges, two approaches to incorporate GO into the BC network were explored.

With the first approach, at lower concentrations (0.5 and 2 mg/mL) of GO dispersed in DI water, BC pellicle was formed at the air-liquid interface while GO nanosheets settled at the bottom, resulting in no interfacial incorporation of GO in BC. At higher concentrations of GO dispersed in DI water (30 and 50 mg/mL), a fraction of GO was incorporated into the BC network, but the membranes were weak and inconsistent, likely due to reduced fiber formation caused by the antibacterial effects of GO[45]. This method did not achieve homogeneous composites or the desired membrane thickness for higher pressure applications. The major challenge encountered with this approach was the dispersion of GO into the nutrient medium, prompting the exploration of an alternative synthesis approach[40,41].

With the second approach aimed at preparing a stable dispersion of GO into PEG-400. Because PEG-400 has high aqueous solubility and is known to enhance the prolonged stability of GO in HS-medium[41]. PEG-400 was found optimal for preparing a stable dispersion due to its viscosity[46] (70.4 mPa.s and density of 1000.3 Kg m^{-3} at 298 K) falling within the range of the HS medium, ensuring compatibility with the desired dispersion characteristics[47]. The higher molecular weight PEG variants such as PEG-600, PEG-1000, and PEG-2000 exhibit higher viscosity levels and are therefore less suitable for achieving the desired dispersion dynamics within the medium[48]. Conversely, PEG-200, characterized by a lower viscosity, was not suitable to prepare the dispersion[49,50]. After 3 days of incubation, a three-dimensional BC-GO hydrogel with cross-linked network of BC nanofibers was formed at the air-water interface. No leftover GO was observed in the Petri dishes with concentration of 0.5 and 2 mg/mL post-harvesting as the composites were very stable, showed strong resistance in tension and could not be torn apart. However, GO dispersion could be still seen in the Petri dishes with concentration of 30 and 50 mg/mL. Higher GO concentrations inhibited the secretion of fibers and the formation of strong adhesion

between GO and BC. High concentrations of GO have been reported to induce antibacterial properties by interacting with bacterial membranes, causing local perturbations that decrease membrane potential, leading to electrolyte leakage and cell lysis[45,51]. The results were supported by yield and wet thickness analysis discussed in the following section. The membranes harvested from the medium with PEG-dispersed GO were labeled as M 0.0 (pristine-BC), M 0.5 (BC-GO 0.5 mg/mL), M 2.0 (BC-GO 2 mg/mL), M 30 (BC-GO 30 mg/mL), and M 50 (BC-GO 50 mg/mL) for further analysis and characterization.

BC yield and wet thickness

BC-GO composite membranes were harvested every second day of incubation till the 16th day. The addition of GO at concentrations of 0.5 mg/mL and 2 mg/mL resulted in thickness of 4.3 and 4.0 mm respectively, on day 16. The desired thickness of 1.2 mm for the never dried BC-GO composites to be used as free-standing membranes in pressure driven filtration was achieved after 3 days of incubation. During the 1st day of incubation in the growth medium, the cultures experienced a lag phase as they adapted to changing environmental conditions, observed across all GO concentrations. After 12 h, bacteria entered the exponential phase and began generating BC pellicles at the air-media interface. Rapid metabolism during the exponential phase resulted in enhanced glucose absorption after 12 h. At this point, the concentration of GO in the medium defines the formation of composites. HS-medium with 0.5 mg/mL GO showed the highest yield among all concentration ranges, likely because *K. Hansenii* are gram-negative bacteria having lipopolysaccharides on their cell membranes, which favor interactions with GO[52,53]. As a result, further incubation time for new batches were limited to 4 days of incubation. From the wet thickness and yield curve analysis after day 5, the yield values started decreasing, leading to lower wet thickness values.

At higher concentrations of GO (30 mg/mL and 50 mg/mL), the yield decreased from the first day of incubation (Figure 1a), indicating that GO concentration was the rate limiting factor for the production of BC-GO composites. Higher GO concentrations dispersed in PEG, retarded the fiber formation of BC, resulting in lower yields. The addition of GO (30 mg/mL and 50 mg/mL) significantly reduced the wet thickness of the composites from millimeter to submillimeter levels over the different periods of incubation as shown in Figure 1b. At higher concentration ranges, after the exponential phase of growth, the decline in oxygen saturation and glucose uptake is accelerated, resulting in the inhibitory effect on the formation of BC-GO composites. This decline results in lower yield because bacteria cannot cope with the unfavorable conditions and hence, they stop growing.

The synergistic impact of PEG and GO on the overall yield of the BC-GO composites can be elucidated by their effect on the crystallinity of BC. Some studies reported that the crystallization process serves as a rate-limiting step in BC production[54]. To overcome this limitation, water-soluble polymers with negatively charged moieties have been employed as supplements to increase yield by diminishing BC crystallinity. The negatively charged groups prevent aggregation by repulsion and the polymers attach to BC microfibrils via hydrogen bonds[55–57]. However, in the adopted synthesis route for BC-GO composites, GO did not lead to a yield increase, presumably due to a notable rise in HS-medium viscosity caused by PEG. The viscosity of the HS-medium influences the penetration of water-soluble polymers into the BC microfibril matrix. When PEG is introduced into the HS medium, the viscosity decreases to a level where GO remains well-dispersed in the medium without settling at the bottom of the petri dish. This promotes better penetration of GO into the BC fiber network and allows it to access the surface of most BC microfibrils. At higher concentrations, GO nanosheets could be entrapped into the BC network, but the composites did not achieve desired thickness suitable for use as free-standing membranes in pressure-driven filtration. This is because higher concentrations increase the viscosity of the nutrient medium, reducing the movement necessary for the excretion of microfibers. Furthermore, the higher concentration of GO imposes oxidative stress resulting in anti-

Fig. 1 | Impact of GO integration on the growth kinetics of BC measured in terms of yield analysis and wet thickness. a Yield (g/L) measured every 2 days during incubation for GO concentrations of 0.0 (M 0.0), 0.5 (M 0.5), 2 (M 2.0), 30 (M 30), 50 (M 50) mg/mL. **b** Wet thickness measurements of BC-GO composites harvested every 2 days for GO concentrations of 0.0 (M 0.0), 0.5 (M 0.5), 2 (M 2.0), 30 (M 30), 50 (M 50) mg/mL.
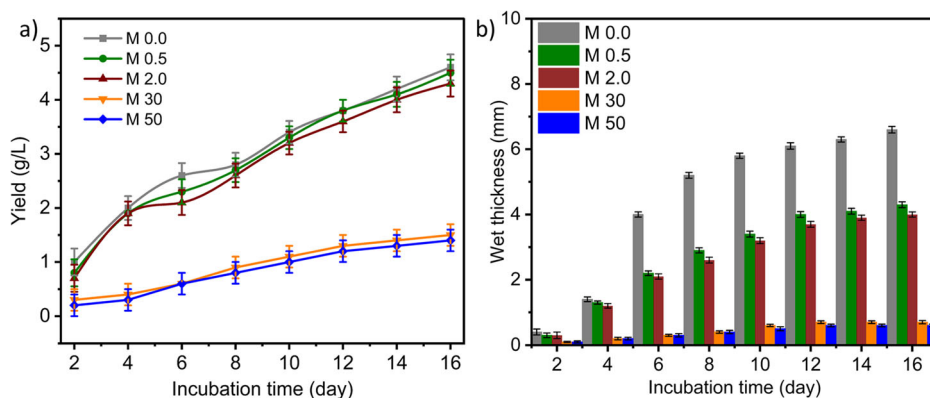
Fig. 2 | Morphological characterization of BC and BC-GO composites. Scanning electron micrographs (SEM) of the surface of (**a**) Pristine-BC (M 0.0) (**b**) BC-GO (M 0.5) composite with 0.5 mg/mL GO concentration (**c**) BC-GO (M 0.5) composite with 0.5 mg/mL GO concentration (**d**) BC-GO (M 2.0) composite with 2.0 mg/mL GO concentration (**e**) BC-GO (M 30) composite with 30 mg/mL GO concentration (**f**) BC-GO (M 30) composite with 30 mg/mL GO concentration. SEM of cross section of (**g**) Pristine-BC (M 0.0) (**h**) BC-GO with 0.5 mg/mL GO concentration (M 0.5) (**i**) BC-GO with 2 mg/mL GO concentration (M 2.0).
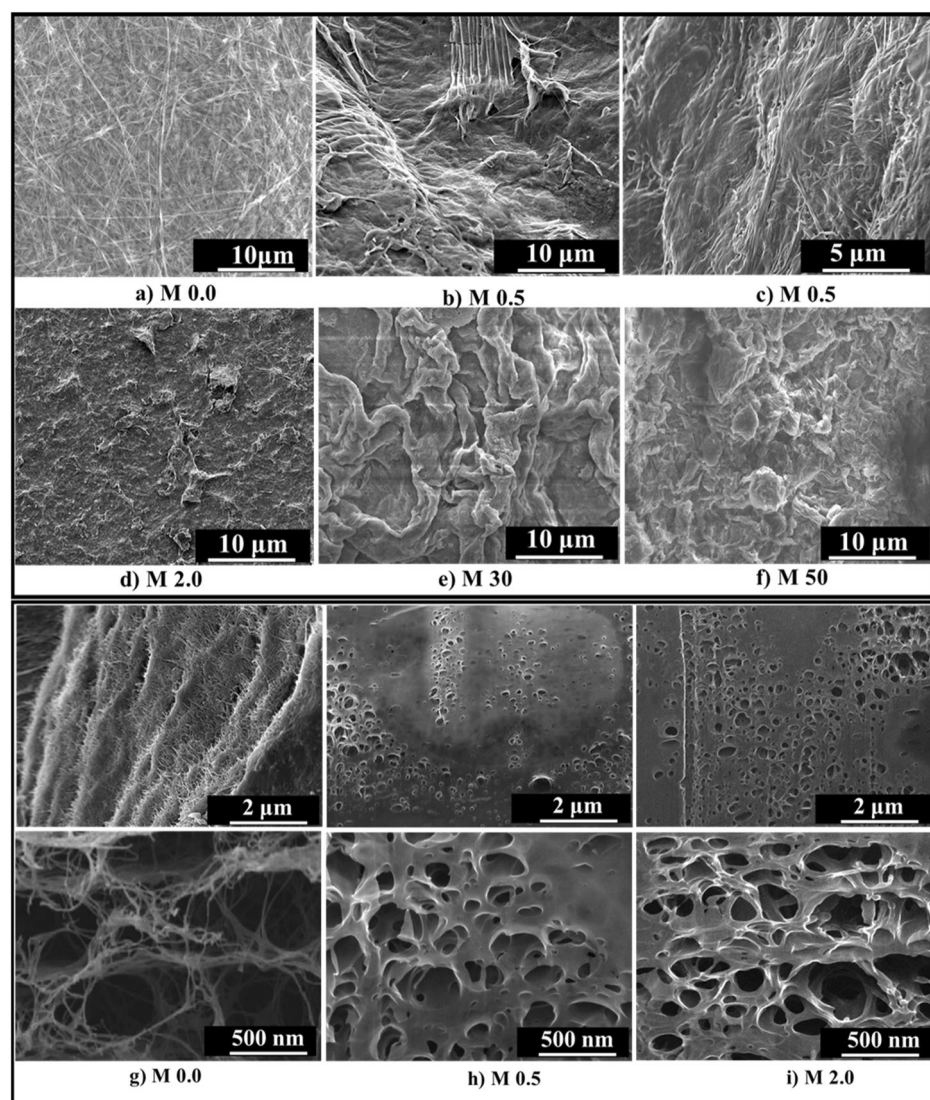

bacterial effect on the inoculum and hence less fiber synthesis and lower yield[58].

Following the yield and wet thickness analysis, some of the composite membranes were dried and used for characterization. However, for evaluating separation performance and fouling behavior, we specifically tested composite membranes with a thickness of 1.2 mm and a GO concentration of 0.5 and 2 mg/mL respectively.

Morphology of BC-GO composites
The pristine-BC films showed highly entangled and continuous fiber layers as shown in Fig. 2a. However, with the incorporation of different concentrations of GO into BC, different morphologies of BC-GO composites were observed. First, at lower GO concentrations (0.5 to 2 mg/mL), the nanosheets were found to be dispersed uniformly in the interlayers of the BC network (Fig. 2b–d). A smooth interface between two materials is formed
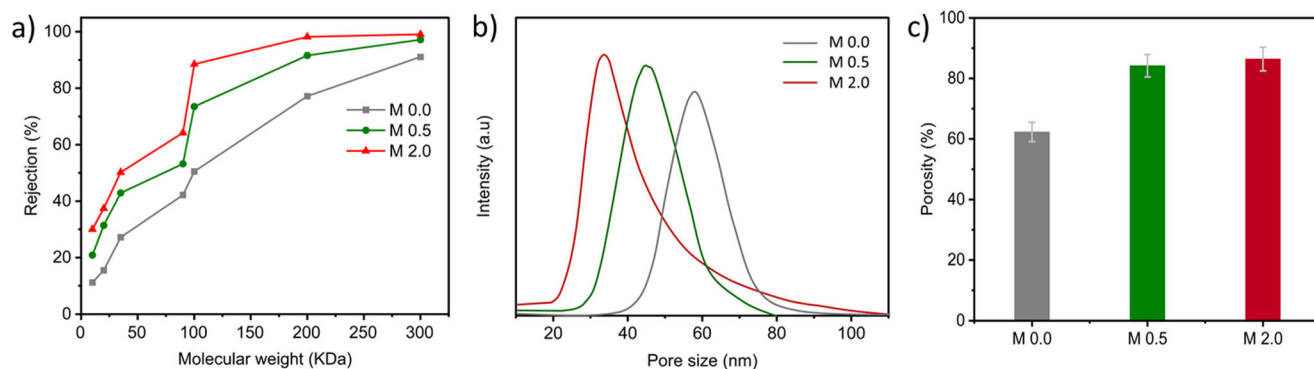
Fig. 3 | Pore size distribution and porosity of composite membranes. a MWCO curve representing rejection of PEG and PEO (**b**) Pore size distribution and mean pore diameter calculated from MWCO method for M 0.0 (Pristine-BC), M 0.5 (BC- GO 0.5 mg/mL), M 2.0 (BC-GO 2 mg/mL) (**c**) Porosity of Pristine-BC and BC-GO composites with a thickness of 1.2 mm and incubation of 4 days.

with the improved interfacial adhesion between two materials brought into by PEG. The interfacial adhesion arises from the intermolecular hydrogen-bonding[59]. The improved dispersion compatibility between HS-medium, GO and PEG arising from intramolecular hydrogen bonding resulted in the effective secretion of BC fibers overlapped and wrapping up the GO nanosheets in between microfibrils. The layer-by-layer thin sheets in BC were seen to be formed that gradually thicken with the increase of cultivation time. This approach of incorporation of GO into different layers supports the interconnection of neighboring GO nanosheets and helps to establish a perforated network-like structure. The perforated structure of BC was also supported by the introduction of porogen, PEG, which was confirmed by the cross-sectional images taken by high intense FIB while cutting across the body of the membrane. Uniform pores, which are not native to the pristine-BC[52], were seen formed throughout the body of the membranes (Fig. 2h,i) for M 0.5 and M 2.0. At higher concentrations of GO (50 mg/mL), the graphene nanosheets were found to be segregated from each other forming isolated patches in the mesh of the BC fibers (Fig. 2f). The patches of GO were seen formed in between the BC fibers, which were not very consistent and uniform. However, at 30 mg/mL, a smaller number of fibers were seen interweaving between the GO nanosheets (Fig. 2e), however agglomerated nanosheets could be observed as well. With retarded formation of fibers, BC membranes were not stable to hold the GO uniformly onto the surface or in bulk.

The changes in morphology observed through SEM micrographs lead to changes in pore morphology and distribution. Figure 3b illustrates the pore size distributions of the pristine and BC-GO composite membranes. The incorporation of GO-PEG into BC matrix affected the average pore diameter and distribution of the resulting BC-GO composites. Specifically, the average pore diameter was reduced from 64 nm in pristine BC to 53 nm (a 17.2% reduction) in BC-GO composites with 0.5 mg/mL GO and further decreases to 42 nm (a 34.4% reduction) in BC-GO composites with 2 mg/mL GO. This reduction in pore size is indicative of the formation of nanopores as GO acts as a nanofiller and fills the larger pores reducing the average pore diameter. Notably, while the average pore diameter is reduced, the BC-GO composites exhibit a broader pore size distribution, ranging from 20 nm to 90 nm, compared to pristine BC. Several studies where high flux and fouling resistance is an important parameter have been reported with broader pore size distribution. Higher flux, fouling resistance and NOM rejection was reported in modified PES ultrafiltration membranes with broader pore size distribution between 10–50 nm and the mean pore diameter of 24 nm[53,60]. Another study reported the broader pore distribution in PEG modified PVDF membrane between 28–135 nm with higher flux and protein purification performance[61]. Because of the natural stacking of sheets in Z direction for Pristine-BC, the pores in between the sheets cannot correspond to each other, resulting in formation of tortuous paths for the fluid flow. The likelihood of a straight-through channel emerging in the Z direction rises as the number of pores in the X-Y direction increases which

results in a reduction in the actual capillary tube length and an improvement in the membrane's flux. As the number of pores increase in the BC-GO composites, the formation of straight through channels increases which results in enhancing the fluid flow through the membranes[62,63]. The results were also supported by an increase in porosity of BC-GO composites compared to Pristine-BC by 32 and 35% for M 0.5 and M 2.0, respectively, as shown in Fig. 3c.
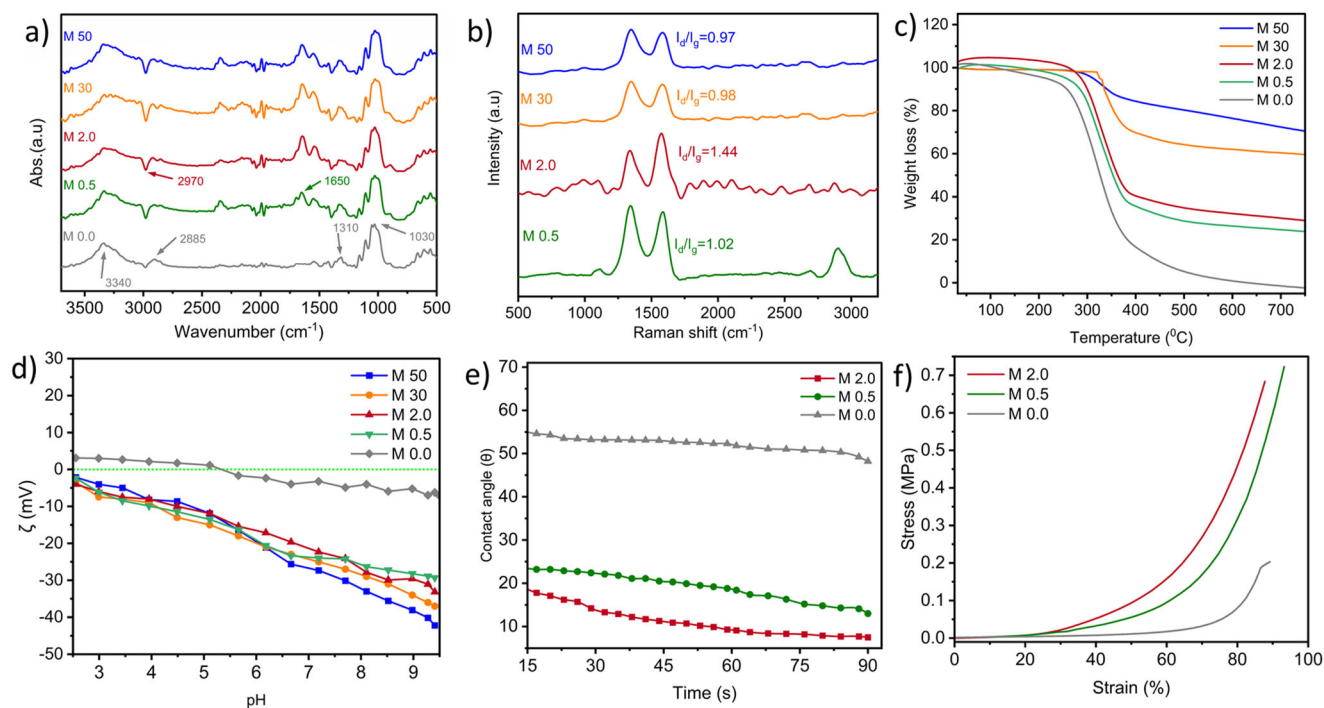
Physicochemical characterization of BC-GO composites

In order to fully understand the effect of GO incorporation on the physicochemical properties of BC, and eventually, to be able to adjust the growth conditions of the composite membranes to improve thermal stability, surface charges and hydrophilicity, chemical characterization of the membranes was carried out.

FT-IR spectra revealed characteristic bands of BC at 3340, 2885, 1650, 1310, 1030 cm^{-1} corresponding to $-OH$ stretching vibrations, $-CH$ asymmetric stretching (CH_2 and CH_3 groups), $-OH$ bending vibrations, CH_2 symmetric bending, and $C–O$ skeletal stretching, respectively[2,64]. The addition of GO into the BC, resulted in significant changes in the spectra (Fig. 4a). The intensity of the band at 3345 cm^{-1} corresponding to stretching vibrations of BC hydroxyl groups, decrease with increasing GO content up to 2 mg/mL. However, at higher GO concentrations, the band remains unaltered, indicating the possible agglomeration of GO[65]. The broadened band at 3371 cm^{-1} in GO-BC composites suggests that the hydrogen bonds in BC have been disturbed. Also, the appearance of a new band at 1650 cm^{-1} representing the antisymmetric stretching vibrations of carboxylate groups, which shows gradual increase in intensity up to 2 mg/mL. This may be due to strong hydrogen bonding interactions between GO and BC[66]. Following this, the band intensity decreases for BC-GO at concentrations of 30 and 50 mg/mL. This decrease confirms that fewer interactions occur between GO and BC at higher concentrations.

Raman spectra of all BC-GO composites showed two distinctive peaks at ~1597 and ~1350 cm^{-1}, consistent with those found in GO, which correspond to the G and D bands of GO, respectively (Fig. 4b)[67]. The D band corresponds to defects in the carbon backbone, and the G band is due to the presence of sp^2 hybridization in graphitic layers. However, GO is not a purely sp^2 system but a highly disordered one with a significant sp^3 content. So, the decrease of defects in GO would produce an increase of the D/G ratio. This is because there would be more sp^2 C atoms surrounding the defects (it is always the sp^2 atoms around, not the defects themselves, which give rise to the D band)[68]. The degree of chemical functionalization in carbon materials can be inferred from the ratio of the intensities of the D and G bands (I_d/I_g); that is, the lower the I_d/I_g ratio, the higher the degree of order of the carbonaceous materials[69]. Both BC-GO composites (0.5 and 2 mg/mL) showed a higher I_d/I_g ratio of 1.02 and 1.44 respectively, suggesting the occurrence of intercalated GO between BC fibers, resulting in increased disorder of the GO sheets[70]. The higher I_d/I_g ratio observed in BC-GO 2 mg/mL indicates better

Fig. 4 | Physicochemical characterization of BC and BC-GO composites of Pristine-BC (M 0.0), BC-GO 0.5 mg/mL (M 0.5), BC-GO 2 mg/mL (M 2.0), BC-GO 30 mg/mL (M 30), BC-GO 50 mg/mL (M 50). a FT-IR spectra of M 0.0, M 0.5, M 2.0, M 30 and M 50. **b** Raman spectra of M 0.5, M 2.0, M 30 and M 50. **c** TGA profile of M 0.0, M 0.5, M 2.0, M 30 and M 50. **d** Streaming potential of M 0.0, M 0.5, M 2.0, M 30 and M 50. **e** Water contact angle (θ) of M 0.5, (M 2.0) with respect to M 0.0. **f** Compression modulus of M 0.0, M 0.5, M 2.0.

interfacial interaction, which leads to the removal of oxygen moieties from GO sheets[71,72]. However, at higher concentrations, the I_d/I_g is low, suggesting less interactions between BC fibers and GO, which correlates with the lower stability of the membranes. M 0.5 showed a peak at 2720 cm^{-1} and ~2931 cm^{-1} corresponding to 2D and D + G bands respectively. The D + G band diminishes with increasing GO concentration which suggests a layered texture of GO in M 0.5 and M 2.0[73].

The effect of GO incorporation on the onset (T_o) and peak degradation (T_p) temperatures and residual ash content (wt %) was evaluated by thermal analysis of the composites (Fig. 4c). The present method for in situ BC-GO biosynthesis demonstrates that GO incorporation greatly enhanced the thermal stability of BC, a phenomenon that was observed at all GO concentrations used. When heated to 200 °C, the pristine BC lost approximately 5% of their weight because of the moisture evaporation, with T_o and T_p being 206 °C and 265 °C, respectively. For all GO concentrations, the BC-GO composites displayed three primary degradation profiles: (i) removal of absorbed moisture due to hydrophilic nature of BC-GO composites; (ii) the onset and peak degradation steps resulting from depolymerization of BC by breaking down the glycosidic bonds; and (iii) release of gaseous products like carbon dioxide or carbon monoxide and presence of solid ash content at temperatures above 400 °C. From the residual ash content analysis, the incorporation of GO lowers the conversion of BC-GO composites into gaseous products and ash content above 400 °C which demonstrates the thermal stability of composites. The residual ash content increased from 0.5% for pure BC to 23%, 28%, 59% and 69% for BC-GO composites (0.5, 2, 30 and 50 mg/mL) respectively. The higher concentration BC-GO composites showed more behavior like GO, an indication of lesser number of fiber formations during in situ biosynthesis. However, for the lower concentration, the effective hydrogen bonding interactions between BC and GO leads to increased thermal stability[74,75].

Electrostatic interactions and surface charge variations of BC-GO composites as a function of pH were evaluated by streaming potential measurements. With the change in pH to the more basic side, all the membranes exhibit negative zeta potential values (Fig. 4d). The surface

charge becomes more negative with the increase of GO concentration in BC with the pristine-BC having a surface charge of −2.3 mV at pH 9. However, the BC-GO composites with concentration of 0.5 and 2.0 mg/mL have the surface charge of −23.1 and −27.2 mV respectively at pH 9. The negative streaming potential is most likely caused by deprotonation of carboxylic acid and hydroxyl groups present on the surface/edges of the BC-GO composites[76,77]. As the pH was increased, the surface charge became more negative which can be ascribed to the ionization of carboxylic acid groups in response to pH changes although a dynamic structure reformation may occur[78]. However, at lower pH values, the surface charge is less negative which is due to the protonation of carboxylic groups on the membranes[79].

The membrane hydrophilicity was elucidated by measuring the water contact angle as shown in Fig. 4e. The lower value of the water contact angle is favored for high membrane hydrophilicity, which can attract more water molecules and thus improve the water flux and antifouling property of the membranes. Herein, GO intercalated between BC layers significantly lowers the contact angle of composite membranes compared with pristine-BC. Pristine-BC has the initial contact angle of 55.4° which decreases with time and reaches a value of 47.2° over a span of 90 s as water is absorbed by the membrane. However, for BC-GO 0.5 and 2 mg/mL composites the initial contact angle values are 24° and 21.3° respectively which eventually decreases to 13.2° and 9.2° making the membranes superhydrophillic. This increased hydrophilicity was attributable to the fact that the hydrophilic functional groups of the GO and PEG were embedded into the membrane which absorb more water and hence lowering the contact angle[80,81].

Mechanical stability of BC-GO composites

The impact of GO and PEG on the compression resilience of BC composites was analyzed by measuring the compressive strength. From Fig. 4f of stress-strain curve, the initial linear region is exhibited. After the linear region, a stress plateau begins to form representing the collapse of structure. Pristine-BC shows the lowest compression modulus of 73 Kpa at 80% compressive strain. BC-GO composites with 0.5 and 2 mg/mL concentration showed more stiffness and increased compressive stress to 315 kPa and 434 kPa
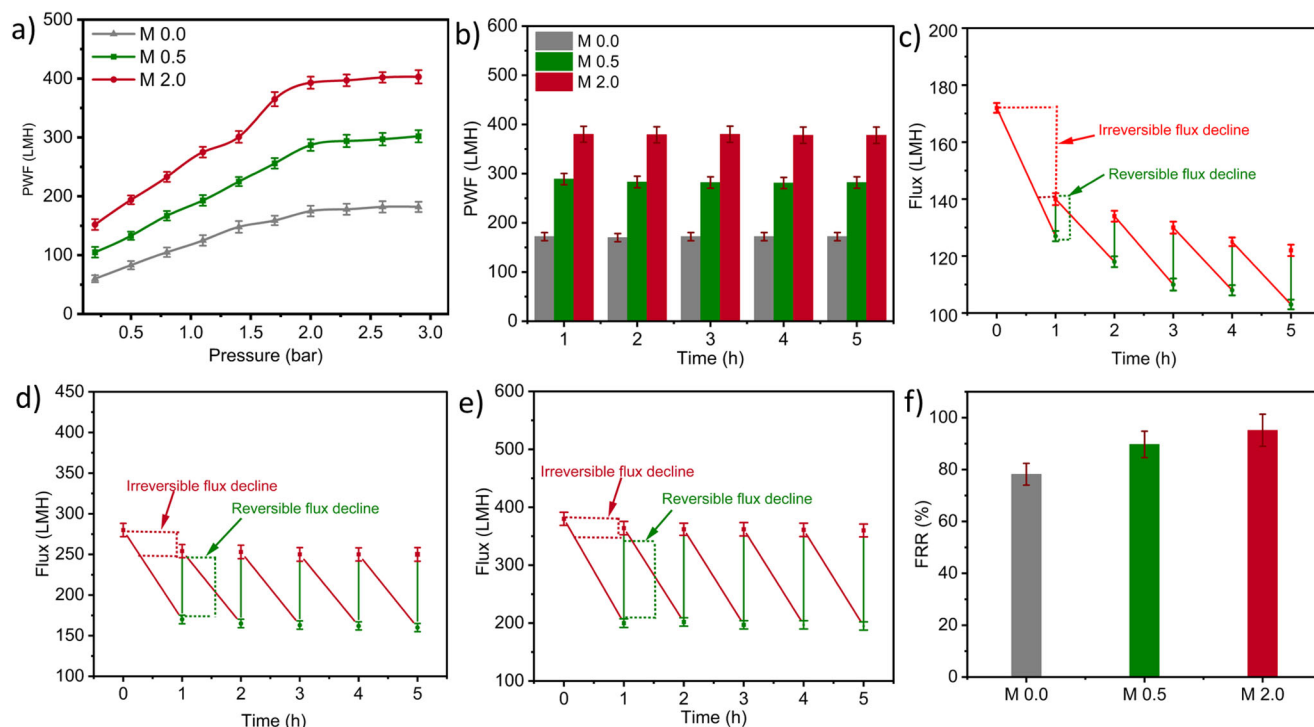
Fig. 5 | Pure water flux, flux decline with NOM and flux recovery. a PWF variation of BC and BC-GO (M 0.0, M 0.5, M 2.0) composites with varying pressure. **b** PWF of M 0.0, M 0.5 and M 2.0 for 5 h. Separation performance with NOM **c** Flux decline with NOM and flux recovery profile of M 0.0. **d** Flux decline with NOM and flux recovery profile of M 0.5. **e** Flux decline with NOM and flux recovery profile of M 2.0. **f** Average flux recovery (%) recorded over five filtration cycles for M 0.0, M 0.5 and M 2.0.

respectively at 80% compressive strain which can be attributed to the stiffness of GO as a reinforcing nanofiller and resilience of PEG which prevents pore collapse of BC. Although the increase in compression strength of BC-GO composites is associated with the incorporation of nanofillers, the behavior of water inside the composites should also be considered. Water does not only bind cellulose chains, but it also binds the nanofillers inside. When membranes are subjected to compression, the water is forced to escape by reducing the volume of membrane under stress. So, the resistance of the incompressible water escaping the membranes plays an important role in compression behavior. BC-GO composites in principle exhibit improved water holding capacity since the added hydrophilic moieties would bind to more water molecules, and hence there will not be complete shrinkage of membrane under an applied compressive stress. Under compressive stresses, water was forced out of each membrane and the compressive strength for BC-GO (2 mg/mL) was found to be fourfold higher than pristine-BC[82,83].

Membrane filtration performance
To investigate the effect of incorporating GO into the BC network, the properties such as PWF, fouling behavior and rejection of microbial pollutants were measured by using three membranes as pristine-BC, BC-GO (0.5 mg/mL) and BC-GO (2 mg/mL) in a cross-flow mode.

The PWF of the membranes was systematically evaluated across a pressure range of 0.1 to 3 bar, as illustrated in Fig. 5a. The membranes showed a linear relationship of flux variation up to 2 bar. However, beyond 2 bar the stability in flux was observed indicating that the maximum compaction had occurred and maximum number of functional pores are open and actively contributing to permeation at this pressure. This behavior is in agreement with the flux variation of hydrogel and never dried BC membranes where a stable flux is reached after maximum compaction has occurred[84,85]. Furthermore, the incorporation of GO into BC enhances the mechanical properties of the composite membrane. GO acts as a reinforcing filler, allowing a greater number of open pores to

remain functional compared to pristine BC membranes, thereby improving overall flux performance. The GO reinforcement not only increases the membrane's structural integrity but also enhances pore interconnectivity as shown in Fig. 2h,i. The better pore connectivity in membranes with the incorporation of GO was reported in polybutylene succinate nanofiber membrane[86] and polysulfone membranes[87]. As a result, BC-GO composites exhibit higher flux in comparison to pristine BC membranes, as GO mitigates pore closure under compression, enabling sustained permeation rates at elevated pressures. Consequently, all subsequent filtration performance assessments were conducted under this established pressure condition of 2 bar. PWF was measured over five filtration cycles each lasting for 1 h as shown in Fig. 5b. BC-GO composite membranes showed higher PWF than pristine-BC. The PWF of pristine-BC was 170.45 LMH which increased to 295.3 LMH for BC-GO (0.5 mg/mL) and finally to 394.56 LMH for BC-GO (2 mg/mL). The increase in PWF was more dominant in BC-GO (2 mg/mL). The increase in flux was attributed to the hydrophilic nature of GO and formation of more nanopores and wider pore size distribution in the BC-GO composites as shown in Fig. 3a. Also GO acts as a nanofiller, which increases the compression resilience of BC-GO composites and helps to keep more pores open when subjected to pressure[83,88]. The PWF for these membranes remained stable over five filtration cycles. The PWF of BC-GO composites was higher in comparison to other reported BC based membranes; for instance, with never dried BC harvested after 5 days of incubation (204 LMH at 2.5 bar)[84]; BC nanopapers flux depending on the grammage of the nanopapers with the highest PWF as 50 LMH Mpa^{-1}[89]; freeze dried BC membranes harvested after 3 days of incubation (52 LMH at 2 bar)[90]. Attempts to prepare BC nanopapers from aqueous dispersions and organic liquids to increase the permeance have been reported with pure water permeance values of 29; 6; 1000; 250 and 100 LMH Mpa^{-1} lower than the BC-GO composites prepared by in-situ synthesis[89,91,92]. BC-GO composite membranes showed improved PWF and stability in comparison to other commercial ultrafiltration membranes such as
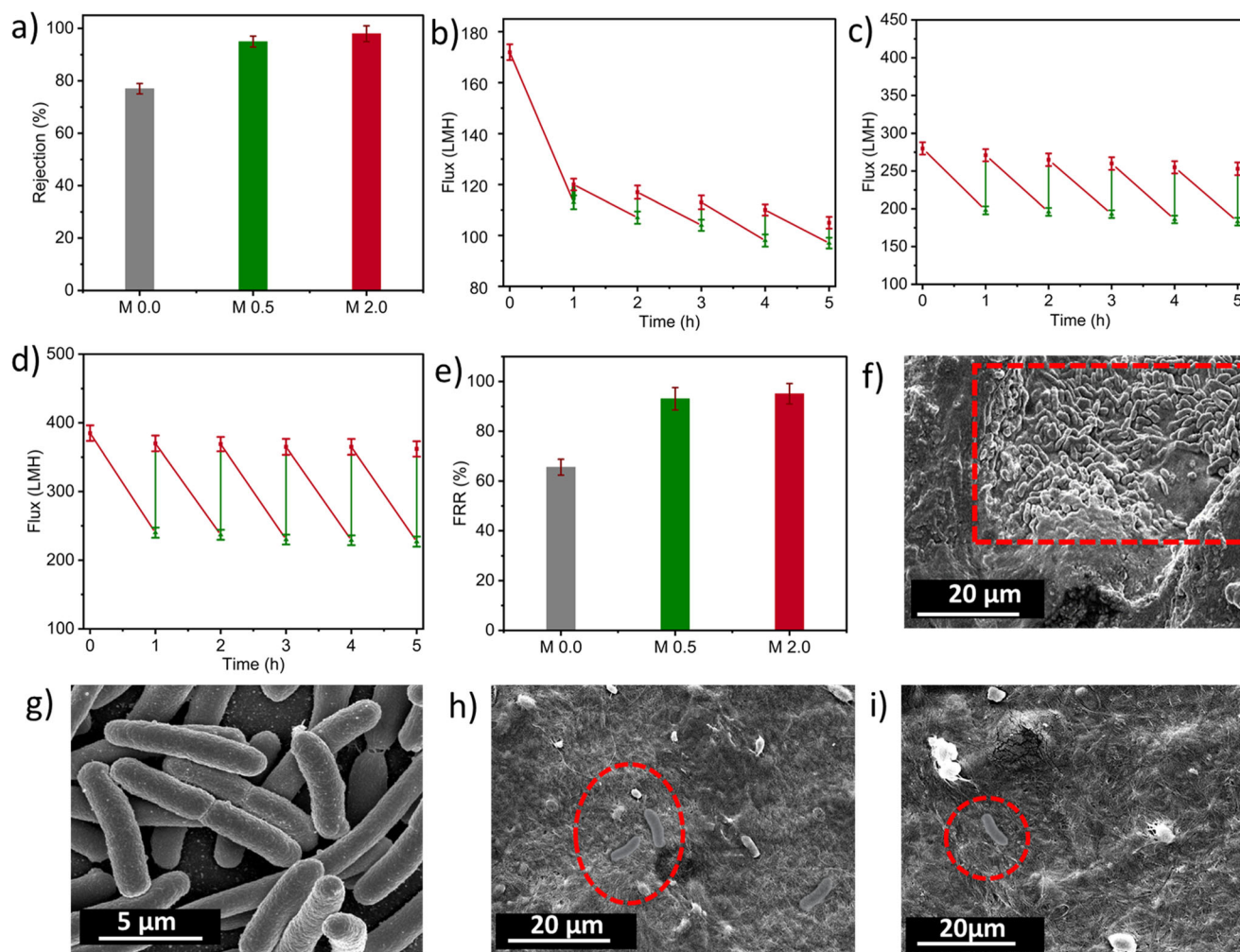
Fig. 6 | NOM rejection, flux profile with bacterial solutions and post filtration morphology. a Rejection of NOM for M 0.0, M 0.5 and M 2.0. **b** Flux decline and recovery with bacteria for M 0.0 (Pristine-BC). **c** Flux decline and recovery with bacteria for M 0.5 (BC-GO 0.5 mg/mL). **d** Flux decline and recovery with bacteria for M 2.0 (BC-GO 2 mg/mL). **e** Average flux recovery (%) after cleaning with DI water. SEM micrographs after filtration and cleaning with DI water representing effective cleaning and reusability. **f** Colonies of E.coli on the surface of M 0.0 (pristine-BC). **g** E.coli colonies on Pristine-BC with higher resolution. **h** Fewer E.coli laying on the surface of M 0.5 (BC-GO 0.5 mg/mL) **i** Single E.coli on the surface of M 2.0 (BC-GO 2 mg/mL).

cellulose acetate, polyamide and polyacrylonitrile with pure water permeability values of 46.06, 24.59 and 80.34 LMH bar^{-1} and working pressure of 2, 4 and 6 bar respectively[93].

Fouling behavior of the membranes was evaluated in a cross-flow filtration mode as described in experimental section. NOM was used as a feed solution for the membranes. The permeate was collected after every hour. The drop in flux of the membranes was recorded over 1 h. The membranes were cleaned with DI water by allowing the water to flow across the membrane surface and erode the NOM layers deposited on the membranes. After every hour of NOM filtration and subsequent cleaning, the PWF was recorded again to calculate the flux recovery of membranes. Pristine-BC had an average flux recovery of 77% while as the flux recovery for BC-GO (0.5 mg/mL) and BC-GO (2 mg/mL) were 89% and 95% respectively (Fig. 5f). It can be seen from the Fig. 5c that the pristine-BC showed an immediate decline in flux after 2nd filtration cycle while as for BC-GO composites the recovery of flux was stable. The PWF of pristine-BC decreased from 173 LMH in the first cycle to 123 LMH in the 5th cycle of filtration. However, for BC-GO (0.5 mg/mL) the PWF had a minimal decrease from 280 LMH in the 1st cycle to 267 LMH in the 5th cycle (Fig. 5d). Similarly, BC-GO (2 mg/mL) membrane had the least decline of flux as shown in Fig. 5e from 390 LMH in the 1st cycle to 386 LMH in the 5th cycle. The improved anti-fouling properties observed in BC-GO composite

membranes can be explained through the synergistic effect of several factors. Primarily, the super hydrophilic nature of the BC-GO surface contributes significantly to its anti-fouling efficacy by forming a dense aqueous layer, which acts as a barrier against the attachment of foulants such as organic matter, and microorganisms. This hydrated layer creates both steric hindrance and an energetic barrier, impeding the adsorption and deposition of foulants onto the membrane surface[94–97]. Several studies reported the change in membrane surface morphology and wettability resulting in the formation of a strong hydration layer; for instance, GO incorporated in PVDF membrane increased the flux recovery from 40.2% to 95.3%[98,99]. However, GO as a nanofiller embedded in commercial polyether sulfone (PES) membranes demonstrated a maximum flux of 70 LMH at 5 bar and a flux decline of 14% less than the pristine-PES membrane[100]. From the streaming potential measurements shown in Fig. 4d, BC-GO composites exhibit significantly more negative surface charges compared to pristine BC. This increase in negative surface charge density increases the repulsion against the negative charged foulants, thereby mitigating their deposition onto the membrane surface. Consequently, the electrostatic repulsion between the membrane surface and the foulants impedes their adhesion, leading to the observed reduction in fouling propensity. Moreover, the enhanced negative charge density enhances the electrokinetic energy barrier, facilitating the efficient removal of foulants during flux recovery processes.
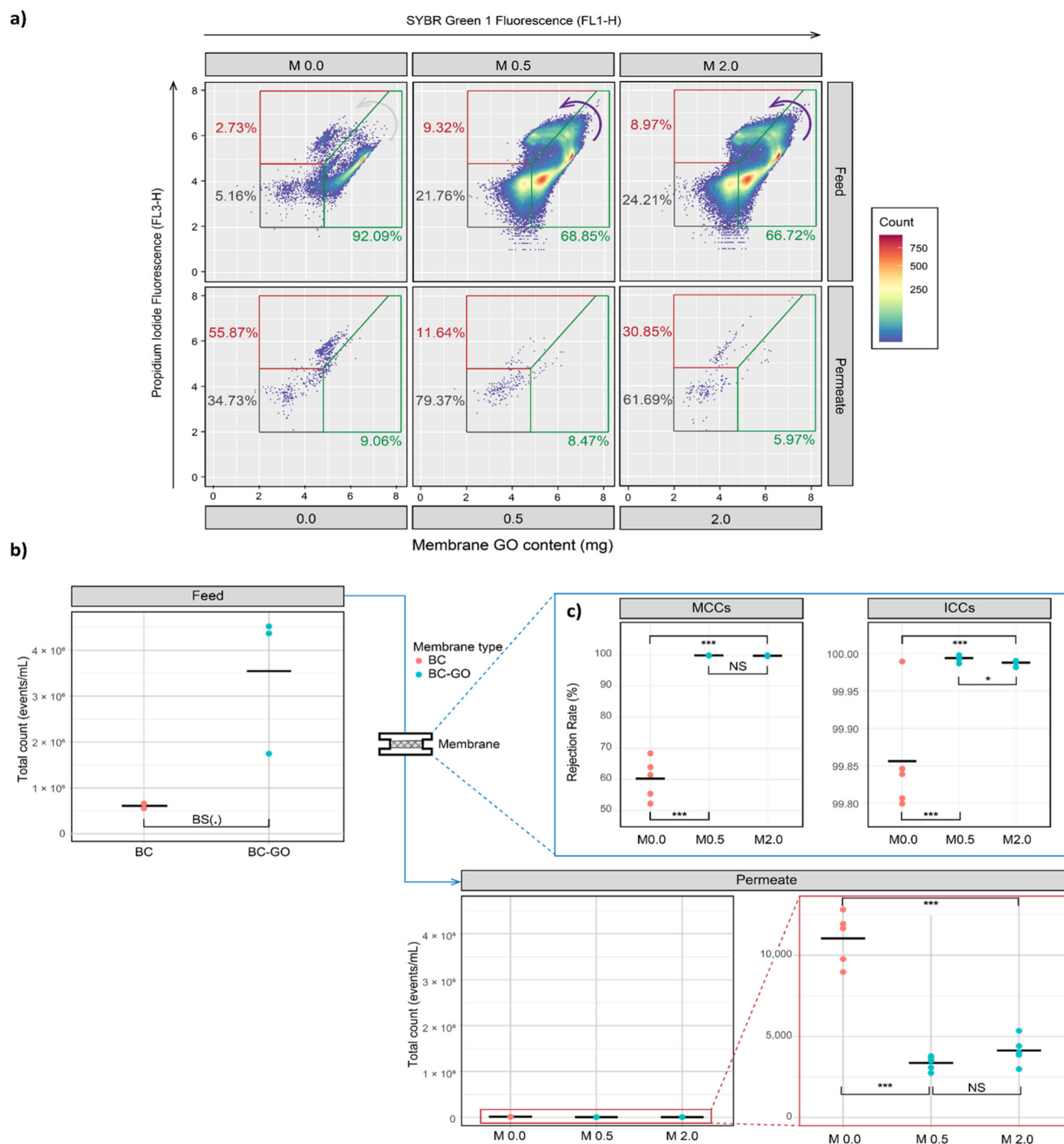
Fig. 7 | Flow cytometry analysis of feed and permeate samples. a Flow cytometry density plots and % count showing E. coli populations (live and dead cells) in the feed and permeate samples for Pristine-BC and BC-GO membranes with 0.0, 0.5, and 2.0 mg/mL GO concentrations. **b** Quantitative analysis for total count of E. coli populations in the feed. **c** % reduction of E.coli population after filtration with M 0.0, M 0.5 and M 2.0 membranes in terms of membrane compromised cell counts (MCCs), intact cell counts (ICCs), and total count in permeate, illustrating the effect of varying GO concentrations on E. coli rejection efficiency.

The synergistic effects of the stacking of BC layers promotes the formation of tortuous channels which increase the dispersion of GO and PEG on the membrane surface and within the BC matrix. PEG contributes to the anti-fouling properties of the membranes through its chain mobility, excluded volume effect, and osmotic repulsion, which collectively aid in the formation of a protective layer on underlying surfaces[101,102]. Ultimately, the presence of this loosely adhered foulant layer on the surface can be removed easily by shear flow cleaning.

Bacteria filtration performance

Removing of harmful pathogenic bacteria is vital for public health in various applications, including drinking water treatment, healthcare settings to prevent infections, and industrial processes where maintaining sterility is critical. The filtration of bacteria-rich broth using pristine-BC and BC-GO composite membranes was investigated with diluted *E. Coli* (1×10^8 colony-forming units (CFU) per milliliter) as the feed solution in cross-flow filtration mode. In comparison to pristine BC membranes, BC-GO composite membranes demonstrated lower flux reduction and stable bacterial

rejection over the course of five filtration cycles. After membrane cleaning, pristine-BC showed 78.2% average flux recovery for five filtration cycles, in line with previous fouling investigations with NOM, whereas BC-GO composites (0.5 mg/mL) and BC-GO (2 mg/mL) demonstrated flux recovery of 89.72% and 95.6% respectively as shown in Fig. 6d. The superior anti-biofouling properties of BC-GO composites were attributed to strong negative charges and the formation of a hydration layer on the membrane surface, hindering bacterial adhesion and facilitating enhanced flux recovery.

The feed and permeate samples collected after hourly intervals were enumerated for *E. coli* as shown in Fig. 7a, b using flow cytometry to evaluate the effectiveness of bacterial rejection. Flow cytometry (FCM) has emerged as a promising alternative to the traditional plate counting method (PCM) for water quality assessment. FCM offers rapid, comprehensive quantification of bacterial communities, contrasting with PCM's limited scope. FCM boasts reproducibility, swift results (within 10 min), and potential cost advantages over PCM. Numerous studies affirm FCM's reliability in tracking total (TCC) and intact (ICC) cell concentrations, pivotal for monitoring efficiency of water treatment systems[103,104]. The log reduction values of bacterial rejection were calculated from flow cytometry analysis where BC-GO composite membranes showed a log reduction of five corresponding to the rejection of 99.99% of the microbial population whereas pristine-BC showed a log reduction of 4. Interestingly, as shown in Fig. 7c BC-GO membranes showed signs of antimicrobial activity in feed water populations (as evidenced by transitionary populations between live and dead cell gates), suggesting a further added merit of integrating GO into BC membrane. The rejection of *E. coli* was significantly enhanced in BC-GO membranes with especially notable declines (<30%) in MCC populations vs BC membranes (*p* < 0.001), likely as a consequence of the antimicrobial activity of GO. Additionally, the rejection of *E. coli* can be ascribed to a size sieving process given the lower pore size of the membranes in comparison to the size of *E. coli*. This outcome was well correlated to the mean pore size of the membranes, which was smaller than the size of *E. coli* mean diameter (0.5 × 1.5 μm), supporting direct size exclusion[105]. A study reported removal of 93.6% removal of microbial pollutants from sea water by surface coating of cellulose membranes with GO nanosheets, however a 6% increase in transmembrane pressure (TMP) was observed compared to 55% increase with pristine cellulose[106].

Pristine-BC and BC-GO composites were cleaned by means of shear flow in the same filtration cell and post-filtration analysis of the membranes was evaluated by SEM analysis. Pristine BC membranes exhibited a notable accumulation of *E. coli* clusters on their surfaces as shown in Fig. 6f, g correlating with reduced flux post-filtration, indicative of significant biofouling. In contrast, BC-GO composite membranes displayed significantly fewer adherent bacteria, often seen as individual bacteria and not in large clusters as for the pristine-BC, as shown in Fig. 6h, i. The flux recovery of the BC-GO composites, which was only achieved with a simple deionized water rinsing, highlights the facile cleanability, and the low-fouling potential of the composite membranes. This behavior may be attributed to the formation of a hydration layer, offered by the presence of the GO, that impedes very strong bacterial adhesion. These findings highlight the potential of BC-GO composites for applications where mitigating biofouling is crucial or where biofilm formation cannot be mitigated through harsh chemical cleaning[107].

A performance comparison table for the membranes based on cellulose and GO reported in the literature is presented in Supplementary Table 1. BC-GO composites showed better flux recovery when water was used as a cleaning liquid instead of chemical washing and treatment reported for removal of foulants such as HA and BSA[108]. With PWF of 290 and 392 LMH, and FRR of 93.4% and 95.7%, respectively, BC-GO membranes showed enhanced permeation compared to BC and GO based membranes reported in the literature[84]. A study reported pure BC membranes grown for 3-day incubation period exhibited a flux recovery of 85.51% with PWF of 52 LMH at 2 bar when BSA was used as a foulant. GO based membranes such as GO blended with commercial PVDF and GO-Polyamide composite membranes demonstrated PWF of 104.3 LMH and 3.5 LMH respectively. When only BSA was used as foulant these membranes showed a flux recovery of 90.5% and 91.4%, respectively[98,109]. In comparison to Cellulose acetate (CA) membrane reported to have flux recovery of 69.3% and PWF of 70.9 LMH at a pressure of 2.75 bar, BC-GO composites in this study showed better permeance and reuse potential[110]. NaClO has been reported to clean *E. coli* fouled membranes, which reacts with membrane materials and *E. coli* cells, leading to the changes in membrane characteristics and the generation of halogenated by-products[111]. However, the membranes developed in this work demonstrated the self-cleaning ability due to formation of strong hydration layer when *E.coli* broth was filtered leading to flux recovery of 95.3%. Furthermore, the inherent antimicrobial properties of GO as reported in the literature, such as its ability to disrupt bacterial cell membranes through physical interaction and oxidative stress, likely contributes to the reduced bacterial attachment observed[112]. Additionally, operating at a low pressure of 0.2 MPa, the membranes demonstrate higher efficiency and lower energy consumption compared to alternatives requiring higher pressures, such as cellulose acetate and other GO based membranes[109,113,114]. These attributes make these membranes ideal for high-throughput and cost-effective applications of membrane filtration.

The findings presented herein hold significant promise for the development of eco-friendly membrane technologies tailored for industrial wastewater treatment §applications. By harnessing the synergistic properties of GO and BC, these membranes offer a sustainable pathway towards the fabrication of high-performance membranes with superior mechanical strength, enhanced permeability, and anti-fouling properties. Additionally, future studies can further explore the biosynthesis of these membranes by evaluating optimized conditions for biosynthesis and microbial growth kinetics. As such, this research contributes valuable insights towards the advancement of greener and more efficient solutions for addressing challenges in wastewater treatment and environmental sustainability.

Data availability

All data generated or analyzed during this study are included in this published article, and its supplementary information files.

References

1. Li, Z., Yang, J. & Loh, X. Polyhydroxyalkanoates: opening doors for a sustainable future. *NPG Asia Mater* **8**, e265 (2016).
2. Gao, M. et al. A natural in situ fabrication method of functional bacterial cellulose using a microorganism. *Nat. Commun.* **10**, 437 (2019).
3. Rahman, S. S. A. et al. Production of bacterial cellulose using Gluconacetobacter kombuchae immobilized on Luffa aegyptiaca support. *Sci. Rep.* **11**, 2912 (2021).
4. El-Naggar, N. E. A., Mohammed, A. B. A. & El-Malkey, S. E. Bacterial nanocellulose production using Cantaloupe juice, statistical optimization and characterization. *Sci. Rep.* **13**, 51 (2023).
5. Walker, K. T. et al. Self-pigmenting textiles grown from cellulose-producing bacteria with engineered tyrosinase expression. *Nat. Biotechnol.* https://doi.org/10.1038/s41587-024-02194-3 (2024).
6. Gorgieva, S. & Trček, J. Bacterial Cellulose: Production, Modification and Perspectives in Biomedical Applications. *Nanomaterials (Basel)* **9**, 1352 (2019).
7. Gregory, D. A. et al. Bacterial cellulose: a smart biomaterial with diverse applications. *Mater. Sci. Eng. R Rep.* **145**, 100623 (2021).

8. Gilbert, C. et al. Living materials with programmable functionalities grown from engineered microbial co-cultures. *Nat. Mater.* **20**, 691–700 (2021).

9. Mir, I. S. et al. Removal of cadmium and chromium heavy metals from aqueous medium using composite bacterial cellulose membrane. *Chem. Eng. J.* **490**, 151665 (2024).

10. Nakayama, A. et al. High mechanical strength double-network hydrogel with bacterial cellulose. *Adv. Funct. Mater.* **14**, 1124–1128 (2004).

11. Mishra, S. et al. Biochemistry, synthesis, and applications of bacterial cellulose: a review. *Front. Bioeng. Biotechnol.* **10**, 780409 (2022).

12. Yousefi, N., Lu, X., Elimelech, M., & Tufenkji, N. Environmental performance of graphene-based 3D macrostructures. *Nat. Nanotechnol.* **14**, 107–119 (2019).

13. Poulin, P. et al. Superflexibility of graphene oxide. *Proc. Natl. Acad. Sci. USA* **113**, 11088–11093 (2016).

14. Chong, J. Y., Wang, B., Mattevi, C. & Li, K. Dynamic microstructure of graphene oxide membranes and the permeation flux. *J. Memb. Sci.* **549**, 385–392 (2018).

15. He, L. et al. Promoted water transport across graphene oxide-poly(amide) thin film composite membranes and their antibacterial activity. *Desalination* **365**, 126–135 (2015).

16. Wei, W. et al. Kozeny-Carman constant of porous media: Insights from fractal-capillary imbibition theory. *Fuel* **234**, 1373–1379 (2018).

17. Zhang, H. et al. In situ controllable fabrication of porous bacterial cellulose. *Mater. Lett.* **249**, 104–107 (2019).

18. Sanei, Z., Ghanbari, T. & Sharif, A. Polyethylene glycol-grafted graphene oxide nanosheets in tailoring the structure and reverse osmosis performance of thin film composite membrane. *Sci. Rep.* **13**, 16940 (2023).

19. Nagasaki, Y. Construction of a densely poly(ethylene glycol)-chain-tethered surface and its performance. *Polymer J.* **43**, 949–958 (2011).

20. Xi, J. et al. High-flux bacterial cellulose ultrafiltration membrane with controllable pore structure. *Colloids Surf. A Physicochem. Eng. Asp.* **656**, 130428 (2023).

21. Lee, Y. H. & Seo, D. S. Toxicity of humidifier disinfectant polyhexamethylene guanidine hydrochloride by two-week whole body-inhalation exposure in rats. *J. Toxicol. Pathol.* **33**, 265–277 (2020).

22. Voisin, H., Bergström, L., Liu, P. & Mathew, A. P. Nanocellulose-based materials for water purification. *Nanomaterials* **7**, 57 (2017).

23. Yin, N., Stilwell, M. D., Santos, T. M. A., Wang, H. & Weibel, D. B. Agarose particle-templated porous bacterial cellulose and its application in cartilage growth in vitro. *Acta Biomater.* **12**, 129–138 (2015).

24. Fang, Q., Zhou, X., Deng, W., Zheng, Z. & Liu, Z. Freestanding bacterial cellulose-graphene oxide composite membranes with high mechanical strength for selective ion permeation. *Sci. Rep.* **6**, 33185 (2016).

25. Udoetok, I. A., Dimmick, R. M., Wilson, L. D. & Headley, J. V. Adsorption properties of cross-linked cellulose-epichlorohydrin polymers in aqueous solution. *Carbohydr. Polym.* **136**, 329–340 (2016).

26. Mota, L. O. & Gimenez, I. F. Cellulose-based materials crosslinked with epichlorohydrin: a mini review. *Revista Virtual de Quimica.* **15**, 2023.

27. Nasution, H. et al. Hydrogel and effects of crosslinking agent on cellulose-based hydrogels: a review. *Gels* **8**, 568 (2022).

28. Zhang, Z., Liu, Y., Lin, S. & Wang, Q. Preparation and properties of glutaraldehyde crosslinked poly(vinyl alcohol) membrane with gradient structure. *J. Polym. Res.* **27**, 228 (2020).

29. Pandey, R. P. et al. Enhanced water flux and bacterial resistance in cellulose acetate membranes with quaternary ammoniumpropylated polysilsesquioxane. *Chemosphere* **289**, 133144 (2022).

30. Tang, L. et al. Bottom-up synthesis of large-scale graphene oxide nanosheets. *J. Mater. Chem.* **22**, 5676 (2012).

31. Smith, A. T., LaChance, A. M., Zeng, S., Liu, B. & Sun, L. Synthesis, properties, and applications of graphene oxide/reduced graphene oxide and their nanocomposites. *Nano Mater. Sci.* **1**, 31–47 (2019).

32. Sutariya, B. & Karan, S. A realistic approach for determining the pore size distribution of nanofiltration membranes. *Sep. Purif. Technol.* **293**, 121096 (2022).

33. Ren, J., Li, Z. & Wong, F. S. A new method for the prediction of pore size distribution and MWCO of ultrafiltration membranes. *J. Memb. Sci.* **279**, 558–569 (2006).

34. Kumar, M., Sreedhar, N., Jaoude, M. A. & Arafat, H. A. High-flux, antifouling hydrophilized ultrafiltration membranes with tunable charge density combining sulfonated Poly(ether sulfone) and aminated graphene oxide nanohybrid. *ACS Appl Mater. Interfaces* **12**, 1617–1627 (2020).

35. Koetzsch, S. Determining the total cell count and ratios of high and low nucleic acid content cells in freshwater using flow cytometry. *Analysis Method.* **333** (2012).

36. McElhinney, J. M. W. R. et al. Computational flow cytometry of planktonic populations for the evaluation of microbiological-control programs in district cooling plants. *Sci. Rep* **10**, 13299 (2020).

37. Hahne, F. et al. flowCore: A Bioconductor package for high throughput flow cytometry. *BMC Bioinforma.* **10**, 106 (2009).

38. Finak, G. et al. OpenCyto: an open source infrastructure for scalable, robust, reproducible, and automated, end-to-end flow cytometry data analysis. *PLoS Comput. Biol.* **10**, e1003806 (2014).

39. R Core Team. *R: A Language and Environment for Statistical Computing [The R Project for Statistical Computing]*. (2024).

40. RStudio Team. *RStudio: Integrated Development for R [Computer Software]*. RStuio, Inc., (2015).

41. Stumpf, T. R., Yang, X., Zhang, J. & Cao, X. In situ and ex situ modifications of bacterial cellulose for applications in tissue engineering. *Mater. Sci. Eng. C* **82**, 372–383 (2018).

42. Moradali, M. F. & Rehm, B. H. A. Bacterial biopolymers: from pathogenesis to advanced materials. *Nat. Rev. Microbiol* **18**, 195–210 (2020).

43. R, R. et al. Bacterial nanocellulose: engineering, production, and applications. *Bioengineered* **12**, 11463–11483 (2021).

44. Wang, J., Tavakoli, J. & Tang, Y. Bacterial cellulose production, properties and applications with different culture methods—a review. *Carbohydrate Polymers* **219**, 63–76 (2019).

45. Liu, S. et al. Antibacterial activity of graphite, graphite oxide, graphene oxide, and reduced graphene oxide: membrane and oxidative stress. *ACS Nano* **5**, 6971–6980 (2011).

46. Gómez-Merino, A. I., Jiménez-Galea, J. J., Rubio-Hernández, F. J., Arjona-Escudero, J. L. & Santos-Ráez, I. M. Heat transfer and rheological behavior of fumed silica nanofluids. *Processes* **8**, 1535 (2020).

47. Sequeira, M. C. M., Pereira, M. F. V., Avelino, H. M. N. T., Caetano, F. J. P. & Fareleira, J. M. N. A. Viscosity measurements of poly(ethyleneglycol) 400 [PEG 400] at temperatures from 293 K to 348 K and at pressures up to 50 MPa using the vibrating wire technique. *Fluid Phase Equilib.* **496**, 7–16 (2019).

48. Bae, S., Sugano, Y. & Shoda, M. Improvement of bacterial cellulose production by addition of agar in a jar fermentor. *J. Biosci. Bioeng.* **97**, 33–38 (2004).

49. Gonzalez-Molina, J., Mendonça da Silva, J., Fuller, B. & Selden, C. The extracellular fluid macromolecular composition differentially affects cell-substrate adhesion and cell morphology. *Sci. Rep.* **9**, 8505 (2019).

50. Xing, G. et al. Density and viscosity of polyethylene glycol 400 + 1,2-propanediamine binary mixtures at T = (293.15–318.15) K and spectral analysis. *J. Solut. Chem.* **52**, 263–287 (2023).

51. Zhang, N. et al. Rapidly probing antibacterial activity of graphene oxide by mass spectrometry-based metabolite fingerprinting. *Sci. Rep.* **6**, 28045 (2016).

52. Sokolnicki, A. M., Fisher, R. J., Harrah, T. P. & Kaplan, D. L. Permeability of bacterial cellulose membranes. *J. Memb. Sci.* **272**, 15–27 (2006).

53. Ibrahim, Y. & Hilal, N. Enhancing ultrafiltration membrane permeability and antifouling performance through surface patterning with features resembling feed spacers. *NPJ Clean. Water* **6**, 60 (2023).

54. Cheng, K. C., Catchmark, J. M. & Demirci, A. Effect of different additives on bacterial cellulose production by Acetobacter xylinum and analysis of material property. *Cellulose* **16**, 1033–1045 (2009).

55. Bagnol, R., Grijpma, D., Eglin, D. & Moriarty, T. F. The production and application of bacterial exopolysaccharides as biomaterials for bone regeneration. *Carbohydr. Polym.* **291**, 119550 (2022).

56. Das, R., Lindström, T., Sharma, P. R., Chi, K. & Hsiao, B. S. Nanocellulose for sustainable water purification. *Chem. Rev.* **122**, 8936–9031 (2022).

57. Mishra, R. K., Ha, S. K., Verma, K. & Tiwari, S. K. Recent progress in selected bio-nanomaterials and their engineering applications: an overview. *J. Sci. Adv. Mater. Devices* **3**, 63–288 (2018).

58. Shankar, K. et al. A review on antimicrobial mechanism and applications of graphene-based materials. *Biomater. Adv.* **150**, 213440 (2023).

59. Mensah, A. et al. Sequestration of Pb(II) ions from aqueous systems with novel green bacterial cellulose graphene oxide composite. *Materials* **12**, 218 (2019).

60. Kadadou, D., Arumugham, T., Tizani, L. & Hasan, S. W. Enhanced antifouling and separation capabilities of polydopamine@Ce-MOF functionalized PES ultrafiltration membrane. *NPJ Clean. Water* **7**, 7 (2024).

61. Lin, Y. C., Tseng, H. H. & Wang, D. K. Uncovering the effects of PEG porogen molecular weight and concentration on ultrafiltration membrane properties and protein purification performance. *J. Memb. Sci.* **618**, 118729 (2021).

62. Wen, X. et al. Understanding water transport through graphene-based nanochannels via experimental control of slip length. *Nat. Commun.* **13**, 5690 (2022).

63. Zhang, W. H. et al. Graphene oxide membranes with stable porous structure for ultrafast water transport. *Nat. Nanotechnol.* **16**, 337–343 (2021).

64. Liu, X. et al. Isolation and characterization of bacterial cellulose produced from soybean whey and soybean hydrolyzate. *Sci. Rep.* **13**, 16024 (2023).

65. Suter, J. L. & Coveney, P. V. Principles governing control of aggregation and dispersion of aqueous graphene oxide. *Sci. Rep.* **11**, 22460 (2021).

66. Wang, C., Wu, R., Wang, L. & Wang, X. Multifunctional flexible graphene oxide/bacterial cellulose composite paper platforms for realtime monitoring sweat and strain in wearable devices. *Chem. Eng. J.* **481**, 148390 (2024).

67. Futamura, R. et al. Staggered structural dynamic-mediated selective adsorption of H2O/D2O on flexible graphene oxide nanosheets. *Nat. Commun.* **15**, 3585 (2024).

68. Lee, A. Y. et al. Raman study of D* band in graphene oxide and its correlation with reduction. *Appl. Surf. Sci.* **536**, 147990 (2021).

69. Su, W., Kumar, N., Krayev, A. & Chaigneau, M. In situ topographical chemical and electrical imaging of carboxyl graphene oxide at the nanoscale. *Nat. Commun.* **9**, 2891 (2018).

70. Sánchez-Campos, D., Reyes-Valderrama, M. I., Mendoza-Anaya, D., Escobar-Alarcón, L. & Rodríguez-Lugo, V. Enhanced methodology for graphene oxide transformation: Unraveling the effects of ultrasonication on morphological and structural characteristics. *MRS Adv.* **9**, 743–748 (2023).

71. Nebol'sin, V. A., Galstyan, V. & Silina, Y. E. Graphene oxide and its chemical nature: multi-stage interactions between the oxygen and graphene. *Surf. Interfaces* **21**, 100763 (2020).

72. Korucu, H., Mohamed, A. I., Yartaşı, A. & Uğur, M. The detailed Characterization of graphene oxide. *Chem. Pap.* **77**, 5787–5806 (2023).

73. Luo, H. et al. Layer-by-layer assembled bacterial cellulose/graphene oxide hydrogels with extremely enhanced mechanical properties. *Nanomicro Lett.* **10**, 42 (2018).

74. Kim, H. C., Panicker, P. S., Kim, D., Adil, S. & Kim, J. High-strength cellulose nanofiber/graphene oxide hybrid filament made by continuous processing and its humidity monitoring. *Sci. Rep.* **11**, 13611 (2021).

75. Mohamed, E. N., Abd-Elhamid, A. I., El-Bardan, A. A., Soliman, H. M. A. & Mohy-Eldin, M. S. Development of carboxymethyl cellulose-graphene oxide biobased composite for the removal of methylene blue cationic dye model contaminate from wastewater. *Sci. Rep.* **13**, 14265 (2023).

76. Pedersen, M. L. K., Jensen, T. R., Kucheryavskiy, S. V. & Simonsen, M. E. Investigation of surface energy, wettability and zeta potential of titanium dioxide/graphene oxide membranes. *J. Photochem Photobio. A Chem.* **366**, 162–170 (2018).

77. Zhou, J. et al. Tuning the reactivity of carbon surfaces with oxygen-containing functional groups. *Nat. Commun.* **14**, 2293 (2023).

78. Baskoro, F. et al. Graphene oxide-cation interaction: inter-layer spacing and zeta potential changes in response to various salt solutions. *J. Memb. Sci.* **554**, 253–263 (2018).

79. Gerland, L. et al. pH-dependent protonation of surface carboxylate groups in PsbO enables local buffering and triggers structural changes. *ChemBioChem* **21**, 1597–1604 (2020).

80. Yi, J., Choe, G., Park, J. & Lee, J. Y. Graphene oxide-incorporated hydrogels for biomedical applications. *Polymer J.* **52**, 823–837 (2020).

81. Prydatko, A. V., Belyaeva, L. A., Jiang, L., Lima, L. M. C. & Schneider, G. F. Contact angle measurement of free-standing square-millimeter single-layer graphene. *Nat. Commun.* **9**, 4185 (2018).

82. Tiwary, S.K., Singh, M., Chavan, S.V., & Karim, A. Graphene oxide-based membranes for water desalination and purification. *npj 2D Mater Appl.* **8**, 27 (2024).

83. Caro-Astorga, J., Lee, K. Y. & Ellis, T. Increasing bacterial cellulose compression resilience with glycerol or PEG400 for robuster engineered living materials. *Carbohydr. Polym. Technol. Appl.* **4**, 100245 (2022).

84. Lehtonen, J. et al. Impact of incubation conditions and post-treatment on the properties of bacterial cellulose membranes for pressure-driven filtration. *Carbohydr. Polym.* **251**, 117073 (2021).

85. Eddine, M. A. et al. Large and nonlinear permeability amplification with polymeric additives in hydrogel membranes. *Macromolecules* **55**, 9841–9850 (2022).

86. Sathirapongsasuti, N. et al. Enhancing protein trapping efficiency of graphene oxide-polybutylene succinate nanofiber membrane via molecular imprinting. *Sci. Rep.* **13**, 15398 (2023).

87. Gilioli Tosin, L., Silvestre, W. P. & Baldasso, C. Incorporation of graphene oxide and reduced graphene oxide on the performance of hybrid polysulfone membranes for gas permeation. *Sci. cum Industria* **11**, e231105 (2023).

88. Kouini, B. & Belhamdi, H. Graphene and graphene oxide as nanofiller for polymer blends. in *Carbon Nanostructures* 231–257. https://doi.org/10.1007/978-3-030-30207-8_9 (2019).

89. Mautner, A. et al. Cellulose nanopapers as tight aqueous ultra-filtration membranes. *React. Funct. Polym.* **86**, 209–214 (2015).

90. Guo, Y. et al. Microbial fabrication of cellulose nanofiber-based ultrafiltration membrane: a sustainable strategy for membrane manufacture. *Cellulose* **30**, 5001–5017 (2023).

91. Mautner, A. & Bismarck, A. Bacterial nanocellulose papers with high porosity for optimized permeance and rejection of nm-sized pollutants. *Carbohydr. Polym.* **251**, 117130 (2021).

92. Janesch, J. et al. Mushroom-derived chitosan-glucan nanopaper filters for the treatment of water. *React. Funct. Polym.* **146**, 104428 (2020).

93. Racar, M., Dolar, D., Špehar, A. & Košutić, K. Application of UF/NF/RO membranes for treatment and reuse of rendering plant wastewater. *Process Saf. Environ. Prot.* **105**, 386–392 (2017).

94. Yang, C. et al. Antifouling graphene oxide membranes for oil-water separation via hydrophobic chain engineering. *Nat. Commun.* **13**, 7334 (2022).

95. Maan, A. M. C., Hofman, A. H., de Vos, W. M. & Kamperman, M. Recent developments and practical feasibility of polymer-based antifouling coatings. *Adv. Funct. Mater.* **30**, 2000936 (2020).

96. Vuong, P., McKinley, A. & Kaur, P. Understanding biofouling and contaminant accretion on submerged marine structures. *npj Mater. Degrad.* **7**, 50 (2023).

97. Xiong, Z. et al. Reinforcing hydration layer on membrane surface via nano-capturing and hydrothermal crosslinking for fouling reduction. *J. Memb. Sci.* **644**, 120076 (2022).

98. Chang, X. et al. Exploring the synergetic effects of graphene oxide (GO) and polyvinylpyrrodione (PVP) on poly(vinylylidenefluoride) (PVDF) ultrafiltration Membrane performance. *Appl. Surf. Sci.* **316**, 537–548 (2014).

99. Rahimi, A. & Mahdavi, H. Zwitterionic-functionalized GO/PVDF nanocomposite membranes with improved anti-fouling properties. *J. Water Process Eng.* **32**, 100960 (2019).

100. Karkooti, A. et al. Development of advanced nanocomposite membranes using graphene nanoribbons and nanosheets for water treatment. *J. Memb. Sci.* **560**, 97–107 (2018).

101. Wang, Y. et al. PEG promoted anti-fouling adsorptive membranes with excellent adsorption performance for removal of pharmaceuticals from water. *J. Environ. Chem. Eng.* **11**, 109263 (2023).

102. Xu, F. J. Deciphering the impact of PEG antifouling layer on surface attached functional peptides in regulating cell behaviors. *Chin. Chem. Lett.* **30**, 2051–2052 (2019).

103. Van Nevel, S. et al. Flow cytometric bacterial cell counts challenge conventional heterotrophic plate counts for routine microbiological drinking water monitoring. *Water Res.* **113**, 28214393 (2017).

104. Hoefel, D. Enumeration of water-borne bacteria using viability assays and flow cytometry: a comparison to culture-based techniques. *J. Microbiol. Methods* **55**, 585–597 (2003).

105. Percival, S. L. & Williams, D. W. *Chapter Six - Escherichia coli. in Microbiology of Waterborne Diseases* 2nd edn, 89–117 (2014).

106. Ibrahim, Y. et al. Surface modification of anti-fouling novel cellulose/graphene oxide (GO) nanosheets (NS) microfiltration membranes for seawater desalination applications. *J. Chem. Technol. Biotechnol.* **95**, 1915–1925 (2020).

107. Vrouwenvelder, H. S. et al. Biofouling of membranes for drinking water production. *Desalination* **118**, 157–166 (1998).

108. Gul, A., Hruza, J. & Yalcinkaya, F. Fouling and chemical cleaning of microfiltration membranes: a mini-review. *Polymers* **13**, 846 (2021).

109. Guo, J., Zhang, Y., Chen, F. & Chai, Y. A membrane with strong resistance to organic and biological fouling using graphene oxide and D-tyrosine as modifiers. *Membranes (Basel)* **12**, 486 (2022).

110. Rana, D. et al. Comparison of cellulose acetate (CA) membrane and novel CA membranes containing surface modifying macromolecules to remove pharmaceutical and personal care product micropollutants from drinking water. *J. Memb. Sci.* **409–410**, 346–354 (2012).

111. Cheng, Y. et al. Further understanding NaClO cleaning of bacteria-fouled ultrafiltration membrane: Variation of membrane structure and formation of halogenated by-products. *J. Environ. Chem. Eng.* **12**, 111681 (2024).

112. Hu, C. et al. GO-based antibacterial composites: application and design strategies. *Adv. Drug Deliv. Rev.* **178**, 113967 (2021).

113. Yan, J. et al. Graphene oxide modified polyamide 66 ultrafiltration membranes with enhanced anti-fouling performance. *Membranes (Basel)* **12**, 458 (2022).

114. Ghobadi Moghadam, A. & Hemmati, A. Improved water purification by PVDF ultrafiltration membrane modified with GO-PVA-NaAlg hydrogel. *Sci. Rep.* **13**, 8076 (2023).

Author contributions

I.S.M.: conceptualization, experimental, data curation, visualization, writing-original draft, review and editing. A.R.: conceptualization (chemistry), experimental, review and editing, validation. J.F.: conceptualization (Microbiology), review and editing, validation. J.S.: review and editing. J.M.: data curation, review and editing, validation. S.P. and H.K.: experimental. J.G.: supervision, review and editing. L.D.: conceptualization, validation, resources, supervision, review & editing, administration. Y.M.: conceptualization, validation, resources, supervision, review & editing, administration.

Competing interests

The authors declare no competing interests.

Additional information

Supplementary information The online version contains supplementary material available at https://doi.org/10.1038/s41545-024-00403-9.

Correspondence and requests for materials should be addressed to Ishfaq Showket Mir or Ludovic F. Dumée.

Reprints and permissions information is available at http://www.nature.com/reprints

Publisher's note Springer Nature remains neutral with regard to jurisdictional claims in published maps and institutional affiliations.